https://doi.org/10.5194/egusphere-2026-2481
Preprint. Discussion started: 8 May 2026

Linking hydrological responses in forest ecosystems to atmospheric forcing

Stefano Martinetti[1], James W. Kirchner[2,3], Peter Molnar[1], and Marius G. Floriancic[1,2]

1Department of Civil, Environmental & Geomatic Engineering, ETH Zurich, Zurich, Switzerland
2Department of Environmental System Sciences, ETH Zurich, Zurich, Switzerland
3Swiss Federal Research Institute WSL, Zurich, Switzerland

Correspondence to: Marius G. Floriancic (floriancic@ifu.baug.ethz.ch), Stefano Martinetti (stefano.martinetti@proton.me)

Abstract. Across ecosystems, soil water is replenished by precipitation events and depleted by evapotranspiration. Evapotranspiration is driven by solar radiation and the aerodynamic evaporative demand of the atmospheric boundary layer (E_{aero}). However, vegetation regulates the rate of transpiration through species-specific stomatal closure mechanisms that depend on tree water status, which in turn depends on the tree's water supply and the atmospheric water demand. Therefore, quantifying the effects of precipitation, solar radiation and E_{aero} on tree-mediated water fluxes is challenging. Here we use ERRA, a framework for de-mixing and de-convolving non-stationary system responses to multiple inputs, to quantify how atmospheric forcing affects ecosystem water fluxes and water content dynamics in a mixed beech and spruce forest. The resulting impulse-response functions describe how soil and tree water fluxes respond to three atmospheric forcing (precipitation, solar radiation, E_{aero}). Water contents of soils and trees responded positively and rapidly to precipitation pulses, indicating fast infiltration of precipitation into the soil and net increases in tree water contents. Tree water contents responded more clearly to precipitation inputs than sapflow rates did, suggesting that precipitation primarily reduced transpiration rather than enhancing tree water uptake. Trees responded quickly and strongly to impulses of solar radiation, but their responses to E_{aero} were less distinct, potentially reflecting stomatal closure effects on transpiration. The impulse-response functions reflected species-specific water use strategies and differences in hydraulic capacitance of trees, which buffered root water uptake during periods of high transpiration demand and thus prolonged the refilling of tree water storage after precipitation events. Impulse responses to solar radiation and E_{aero} were much less distinct in the soils than in the trees, illustrating how forest canopies shield the underlying soils from atmospheric forcing. Our study highlights how impulse-response functions can help to identify soil-plant-atmosphere relations, complementing our understanding of forest ecosystem functioning in response to atmospheric forcing.

Summary (500 characters including spaces)

We measured impulse responses of water fluxes to atmospheric forcing in a mixed beech and spruce forest. We found rapid responses to precipitation in soils and trees, and rapid responses to solar radiation and aerodynamic evaporative demand in

https://doi.org/10.5194/egusphere-2026-2481
Preprint. Discussion started: 8 May 2026

trees, but not in soils, which suggests that the forest canopy significantly shielded the soils from atmospheric forcing. We also found impulse-response functions to be affected by species-specific stomatal regulation and hydraulic capacitance.

1 Introduction

Transpiration from terrestrial ecosystems significantly affects the water cycle (Schlesinger and Jasechko, 2014). Transpiration is driven by atmospheric evaporative demand, is limited by soil water availability, and is controlled by species-specific plant physiology, complicating efforts to predict transpiration and its effects on the water cycle. Two key drivers of transpiration are incoming solar radiation, which provides the essential energy for photosynthesis, and the aerodynamic evaporative demand (E_{aero}), determined by wind speed and vapor pressure deficit (VPD; i.e., air dryness). Plant stomata regulate transpiration in response to changes in solar radiation and E_{aero}. As radiation increases, stomata open to gain carbon for photosynthesis. As E_{aero} increases, stomata may close to limit water loss to the atmosphere (Grossiord et al., 2020; McAdam and Brodribb, 2015). During times of high VPD or high solar radiation, stomata continuously adjust to prevent excessive water loss (Brodribb and McAdam, 2011), linked to turgor loss (e.g., Rodriguez-Dominguez et al., 2016) or even cavitation when water potentials approach extremely low values (e.g., Jones and Sutherland, 1991).

Multiple studies in arid or semi-arid regions have found that soil water replenishment following precipitation pulses leads to transient increases in plant growth, transpiration and soil respiration (Collins et al., 2014; Delgado-Balbuena et al., 2023; Huxman et al., 2004a, b; Williams et al., 2009; Zeppel et al., 2008). Similar dynamics are also observed in more humid landscapes, as soil moisture increases after precipitation events, followed by progressive soil drying and decreasing plant and soil microbiome activity (Bai et al., 2026; Feldman et al., 2018). However, these studies have typically been based on daily observations, while plants and soils respond to precipitation inputs and atmospheric controls on much higher temporal resolutions. Furthermore, precipitation, VPD, solar radiation and soil moisture are strongly correlated at both sub-daily and longer timescales (Zhou et al., 2019), making it difficult to isolate their individual effects on plant and soil water fluxes. There are also feedbacks among many of these variables; for example, stomatal closure due to high VPD causes further increase in VPD as a consequence of the reduced water vapor supply from transpiration (Zhou et al., 2019). Similarly, because precipitation recharges soils but simultaneously decreases E_{aero} by raising humidity, its short-term and longer-term effects on transpiration may differ in magnitude or even in sign. To date, attempts to capture the effects of individual controls on transpiration have analyzed isolated periods with different antecedent dryness conditions (Feldman et al., 2021a, b) and cloud cover (Burns et al., 2015).

Here, we explore responses of tree-mediated water fluxes to precipitation, solar radiation and E_{aero} using model-independent, data-driven methods that quantify impulse-response functions of nonstationary systems by de-convolving and de-mixing their input and output time series (Kirchner, 2022). We use the ERRA (Ensemble Rainfall Runoff Analysis, ERRA -- an R script

https://doi.org/10.5194/egusphere-2026-2481
Preprint. Discussion started: 8 May 2026

for Ensemble Rainfall-Runoff Analysis., 2026) framework, which was originally developed to capture runoff responses to precipitation of varying intensity under changing environmental conditions (Kirchner, 2024). ERRA has been successfully applied in combination with transit time distributions (Knapp et al., 2025), to link groundwater recharge to streamflow (Gao et al., 2025b) and to quantify controls on rapid and delayed runoff response (Gao et al., 2025a). Here we use ERRA to obtain impulse-response functions linking precipitation, solar radiation and E_{aero} as ecosystem impulses, and multiple water fluxes and dynamic water states as ecosystem responses. All these ecosystem impulses and responses were measured at sub-hourly resolution over the course of five growing seasons (2021-2025) at the WaldLab study site in Zurich. In particular, we assessed net recharge and depletion of soil and tree water content, net change of soil and branch water potentials, and sapflow dynamics of beech and spruce trees. We hypothesize that data-driven deconvolution of impulse-response relationships with different controls will yield insights into mechanisms affecting ecosystem water fluxes, i.e., variations in stomatal conductance in response to solar radiation or E_{aero} depending on soil water availability. We further hypothesize that species-specific physiological traits will be evident in the estimated impulse-response functions, making ERRA a useful tool for identifying and comparing ecosystem processes across biomes.

2 Materials and Methods

2.1 Field site and measurement setup

The impulse-response analyses presented here are based on atmospheric controls and ecosystem water fluxes measured at the "WaldLab Forest Experimental Site" in Zurich (Switzerland, see Fig. 1). The study site is a typical central European managed mixed beech and spruce forest stand situated on a south-west facing slope. The mean annual temperature is 9.3 °C and annual precipitation averaged 1134 mm between 2010 and 2022. The luvisol soil at the site is roughly 1 m deep covering moraine material. Atmospheric variables were measured with an Atmos 41 all-in-one weather station (Meter Group GmbH) located in a clearing approximately 150 m outside of the forest plot. Soil water contents and soil water potentials were measured within a cluster of beech and a cluster of spruce trees (Fig. 1) every 10 minutes at 10, 20, 40 and 80 cm depth, using Teros 11 & 12 soil moisture sensors and Teros 21 (10, 20 and 40 cm) or Teros 32 (80 cm) matric potential sensors (all sensors from Meter Group GmbH). We also installed eleven Teros 21 sensors at 20 cm depth along a transect between the beech and the spruce clusters. Sapflow was measured at 10-minute resolution in three beech and four spruce trees using SFS2 sapflow sensors (UP GmbH) installed at breast height (see Fig. 1). Sapflow sensor thermocouple readings in mV were converted to temperature difference in °C using a temperature-dependent factor as specified by the manufacturer. Temperature differences were converted to sapflow density using a Granier-type equation (Eq. B1 in Appendix B) with parameters obtained through a joint calibration of beech and spruce data as suggested by Peters et al. (2021), because beech and spruce yielded similar parameter values (see Fig. C1 in Appendix C). Three beech and three spruce trees were equipped with point dendrometers (ZN12 point dendrometers, Natkon AG) that measured stem radius variations at 10-minute resolution (see Fig. 1). We interpret the radius fluctuation signals as changes in tree water deficit (as explained in Zweifel et al., 2005). We transformed tree water deficit into

https://doi.org/10.5194/egusphere-2026-2481
Preprint. Discussion started: 8 May 2026

relative measure of tree water content by inverting the signal (multiplying by -1) and subtracting the smallest measured water content. Thus, the reference level of 0 for relative tree water content corresponds to the largest recorded tree water deficit. Three beech trees and one spruce tree were periodically equipped with psychrometers measuring at 15-minute resolution (PSY1 – ICT International Inc) during dry periods of the 2022, 2023 and 2024 growing seasons (see Fig. 1). Psychrometers had to be removed and re-installed frequently due to measurement failure and therefore could not always be installed on the same branch.

We used these data to quantify impulses of atmospheric forcing by precipitation, vapor pressure deficit and solar radiation, and several resulting ecosystem responses, including changes in soil water content, soil water potential, sapflow density, tree water balances (obtained from dendrometer measurements) and branch water potentials (obtained from psychrometer measurements).

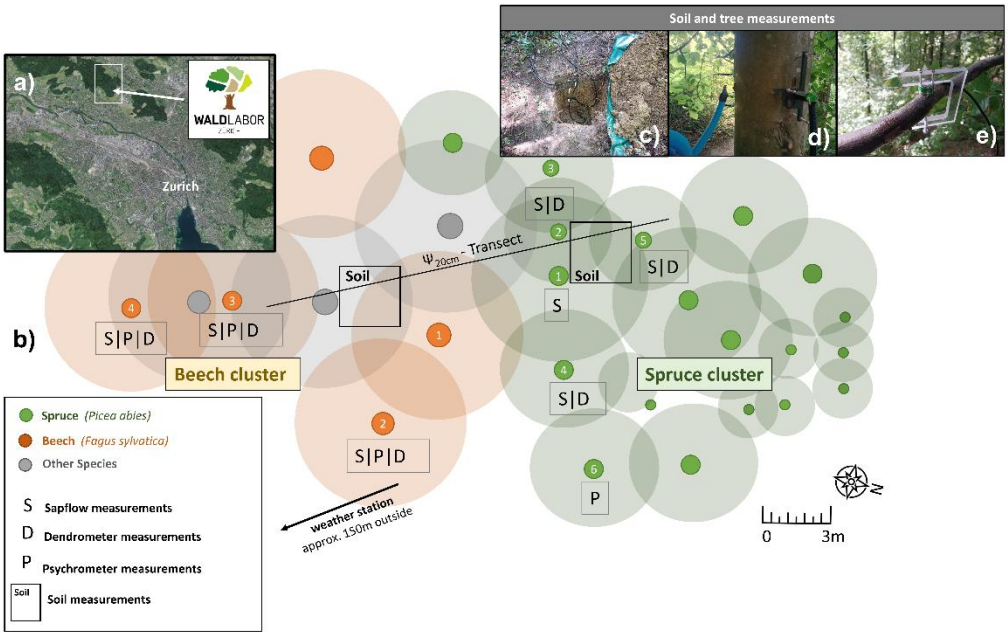

Figure 1: Location of the 'Waldlabor' site in Zurich (a) and a schematic of the "WaldLab Forest Experimental Site" (b), indicating the locations of trees (spruce, beech and other species shown in green, orange and grey, respectively). The trees where sapflow sensors, dendrometers and psychrometers were installed are labelled with S, D and P respectively. Measured and estimated tree properties are shown in Table S1. The locations of the soil water profiles are indicated by black squares. The transect of soil water potential sensors connecting the beech and spruce clusters is indicated by the black line. The weather station is located outside the forest, approximately 150 m from the experimental site. Inset photos in the upper right corner show examples of soil sensor installation (c), sapflow and dendrometer sensor installation on a beech trunk (d), and psychrometer installation on a beech branch (e).

https://doi.org/10.5194/egusphere-2026-2481
Preprint. Discussion started: 8 May 2026

2.2. Applying ERRA to water fluxes and water states measured in soils and trees

ERRA (Ensemble-Rainfall-Runoff-Analysis) facilitates data-driven calculation of impulse-response functions of nonlinear, nonstationary and heterogeneous systems (Kirchner, 2022). ERRA has been used to understand the hydrological behavior of catchments (Kirchner, 2024; Knapp et al., 2025), to compare response times and travel times in hydrology (Knapp et al., 2025), to quantify controls on rapid and delayed runoff responses in double-peak hydrographs (Gao et al., 2025a) and to study ecosystem water fluxes based on soil moisture and flux tower measurements (Gao et al, in press). However, the ERRA methodology can also be adapted to many different impulse–response data sets, as the underlying mathematical foundation is general. The mathematical foundation of the methodology is explained in detail in Kirchner (2022) and the proof-of-concept analyses are presented in Kirchner (2024).

ERRA is based on de-convolving time series of impulses (I) and responses (R) at time j by fitting coefficients (β) for lag times from 0-k time steps between impulses and subsequent responses, yielding a multiple linear regression equation, where α is the constant term and ε_j are the residuals:

$$R_j = \sum_{k=0}^{m} \beta_k I_{j-k} + \alpha + \varepsilon_j \ , \qquad (1)$$

Within ERRA, residuals are assumed to be serially correlated, and ERRA automatically quantifies (and corrects for) serial correlation up to any arbitrary order (Kirchner, 2022). ERRA is further able to consider multiple impulses driving a response by expanding Eq. (1) with additional terms containing the coefficients and impulses of multiple controls. ERRA can quantify impulse-response functions even when the individual impulse time series are correlated (see Kirchner, 2022), as is the case in our dataset, where precipitation, E_{aero}, and solar radiation are strongly correlated. Additionally, the time series used to calculate the impulse-response functions can be subdivided based on user-specified criteria, in order to infer how the system's impulse response might change as ambient conditions change. For example, the response of streamflow to the same amount of precipitation varies for different levels of antecedent wetness (Gao et al., 2025a; Knapp et al., 2025).

Here we extend the application of ERRA from rainfall-runoff assessments to ecosystem water flux responses to impulses from precipitation, aerodynamic evaporative demand (E_{aero}) and solar radiation during WaldLab's main growing season (April to September). The atmospheric impulses are correlated, as precipitation causes E_{aero} to decline and generally occurs with substantial cloud cover and lower solar radiation. Moreover, E_{aero} and solar radiation are strongly coupled due to the strong radiation effect on temperature. The de-mixing capabilities of ERRA provide an opportunity to disentangle the individual effects of these controls on ecosystem water fluxes. The individual response variables were analyzed independently from each other, meaning that ERRA was run independently for each response variable with the same set of impulse variables.

https://doi.org/10.5194/egusphere-2026-2481
Preprint. Discussion started: 8 May 2026

We analyzed the impulse-response functions of the trees up to time lags of 10 hours because this timespan covers the duration of daily periods of transpiration and because most responses were significantly shorter than 10 hours. For response variables measured in the soil, we evaluated the impulse-response functions at a geometric progression of time lags up to 5 days (with ERRA's nk parameter) rather than evenly spaced time lags, because the soil water responses occurred over a wide range of lag times (see Fig. 6&7). We further analyzed how the impulse-response functions vary based on soil water availability. To distinguish between relatively wet and dry soil conditions, we used five-hour average soil water potential measurements at 20 cm depth to subdivide our analysis period into wet soil conditions ($\Psi_{20\ cm}$>-0.5 MPa) and dry soil conditions ($\Psi_{20\ cm}$≤-0.5 MPa), with -0.5 MPa approximating the 0.3 quantile of average soil water potential at 20 cm within the beech cluster, where soils were generally drier compared to the spruce cluster (see Martinetti et al., 2025) and Fig. C3 in Appendix C.

2.3. Data preparation and aggregation

When the inputs and the outputs are provided in the same unit (e.g., mm h^{-1}) to ERRA, the calculated impulse-response functions can be interpreted as distributions in units per time (e.g., h^{-1}), describing the response at a given time lag per unit (increment) of the forcing variable. However, the variables measured at the site are reported in several different units. To facilitate comparisons among the three controls, we express E_{aero} and solar radiation in terms of equivalent water fluxes in mm H_2O h^{-1}. We computed the aerodynamic evaporative demand of the atmosphere (E_{aero}) from terms corresponding to a typical potential evapotranspiration equation:

$$E_{aero} = \frac{\rho_a c_p}{\rho_w \lambda} * g_a * VPD * \Delta t \quad (2)$$

where g_a (the aerodynamic conductance) was derived from wind speed using a logarithmic wind profile and extrapolated to a reference grass surface assuming neutral stability, ρ_a and ρ_w are the air and water densities, respectively (1.002 kg m^{-3} and 998.3 kg m^{-3}), c_p is the specific heat capacity of air at constant pressure (1004 J kg^{-1} K^{-1}), and λ is the latent heat of vaporization (2.45 MJ kg^{-1} at 20°C). E_{aero} represents atmospheric drying power independent of radiative energy constraints and has units of mm H_2O h^{-1}. Solar radiation (originally measured in W m^{-2}) was converted to kg H_2O m^{-2} h^{-1} using λ and ρ_w.

Where possible, we also converted the response variables into units of mm H_2O h^{-1}, taking the derivative in time where necessary. Soil water content expressed as V_{H2O}/V_{soil} was converted to V_{H2O}/A_{soil} (resulting in mm H_2O) using the measured soil volume and footprint around the Teros 11/12 VWC sensors (1010 ml and 66 cm^2). We then took the time derivative of soil water content, to obtain the rate of net soil water recharge in mm H_2O h^{-1}, following Gao et al. (in press). We converted sapflow density into sapflux using the xylem area (estimated from tree cores – see Table A1 in Appendix A), and then converted it to a flux per unit surface area by the area of the tree crown, estimated using the diameter at breast height (see Sharma *et al.*, 2016 and Table A1 in Appendix A), yielding sapflux in mm H_2O h^{-1}. Dendrometer measurements of tree stem

https://doi.org/10.5194/egusphere-2026-2481
Preprint. Discussion started: 8 May 2026

radius (in units of mm) were converted to changes in tree water content by taking the time derivative (to obtain mm h^{-1}), multiplying by estimated circumference of the active xylem (to obtain mm^2 h^{-1}), and scaling by the ratio between tree height and tree crown area (as estimated above) to obtain the net tree water balance (i.e., change in tree water content) per unit crown area, in mm H_2O h^{-1}.

We took the time derivatives of soil and tree water potentials to highlight their dynamic response to changes in atmospheric forcing. We did not attempt to convert these net changes in soil and tree water potentials to mm H_2O h^{-1} because they have no straightforward equivalents in terms of water content. Converting the other variables, however, has the advantage of expressing them in the same dimensions as the atmospheric forcing variables, facilitating more straightforward comparisons. Although some of the conversion factors (such as estimates of xylem area and crown area) are uncertain, they are used only as scaling constants and thus do not affect the dynamics embodied in the impulse-response functions.

All of the response variables except sapflow are measured as states rather than fluxes, and are converted to fluxes or rates of change by taking their derivatives. This facilitates comparisons with the forcing variables by making their dimensions comparable, and by emphasizing the system's dynamic response rather than the persistent change in its state. For example, soil water content typically responds to precipitation impulses by increasing rapidly, followed by an extended period of drying due to evapotranspiration and drainage (see Fig. 2); by contrast, the rate of net soil water recharge (the derivative of soil water content) spikes immediately after the precipitation impulse and then declines toward a near-zero baseline (see Fig. C8 in Appendix C), providing a more sensitive indicator of short-term dynamics, and thus a more suitable signal for quantifying impulse-response functions.

The atmospheric forcing is measured at a single location (the weather station), but tree responses and some soil responses (i.e., soil matric potential at 20 cm depth) were measured using multiple sensors at multiple locations. Averaging these measurements across locations would lead to a loss of data for all time steps in which any location's data is unavailable. Instead, we concatenated the time series for each sensor sequentially, along with stacked copies of the forcing variables, and used these stacked replicate time series as inputs to ERRA (the transitions between each of the sensors occur outside the growing season and thus are ignored by the analysis). The resulting impulse-response functions quantify the average response and its standard error based on all responses at all locations, with the standard error also accounting for the differences in response between different sensors or locations.

We ran ERRA on half-hourly data obtained by aggregating and averaging the 15-minute data from psychrometers and 10-minute data from other sensors. We additionally ran ERRA on daily averages of the soil data. The magnitudes and timings of the obtained impulse-response functions reflect how trees and soils respond to unit step increases of individual atmospheric control variables, while all other atmospheric control variables remain equal.

https://doi.org/10.5194/egusphere-2026-2481
Preprint. Discussion started: 8 May 2026

3. Results and Discussion

3.1. Measured atmospheric forcing, water fluxes and water states in soils and trees

Figure 2 shows example time windows of the measured impulse (Fig. 2a-d) and response variables (Fig. 2e-n) during periods of relatively wet and dry soil conditions (see Fig. C8 in Appendix C for a version of Fig. 2 where the same variables are transformed into mm h^{-1}). Sapflow followed the daily cycles of the two major drivers of transpiration, E_{aero} and solar radiation. However, lower soil water availability during dry soil conditions reduced sapflow for both beech and spruce (Fig. 2i&j). Tree water contents and branch water potentials were inversely linked to sapflow, consistent with high sapflow rates arising in response to low tree water potentials, which in turn arise from tree water deficits. For spruce, tree water content correlated with soil water potentials after re-wetting by precipitation (Fig. 2h&l). Sapflow was higher and tree water content fluctuations were smaller for beech than for spruce, reflecting higher transpiration but smaller internal tree water storage capacity for beech (Fig. 2i-l). Fluctuations in branch water potentials were similar for beech and spruce and were stronger during dry periods (Fig. 2m&n). Visually inspecting the time series suggests that precipitation impulses cause strong, rapid responses in soil water contents and soil water potentials, as well as spruce tree water contents, and that solar radiation and E_{aero} generate strong sapflow responses in both tree species. Overall, responses to precipitation were stronger during dry periods. Sapflow response to E_{aero} and solar radiation was weaker during dry periods, while the response of branch water potential was stronger. However, given the strong correlation between vapor pressure deficit and solar radiation it is difficult from visual inspection only to determine the response to these drivers independently.

During wet and dry soil conditions, precipitation characteristics and solar radiation dynamics remained similar, while E_{aero} increased during dry soil conditions compared to wet soil conditions (Fig. 3). Solar radiation and E_{aero} are strongly correlated on half-hourly time scales (Pearson r=0.44; p<0.001) during the growing season. Half-hourly precipitation is weakly (and negatively) correlated with both E_{aero} (r=-0.07; p<0.001) and solar radiation (r=-0.1; p<0.001).

https://doi.org/10.5194/egusphere-2026-2481
Preprint. Discussion started: 8 May 2026

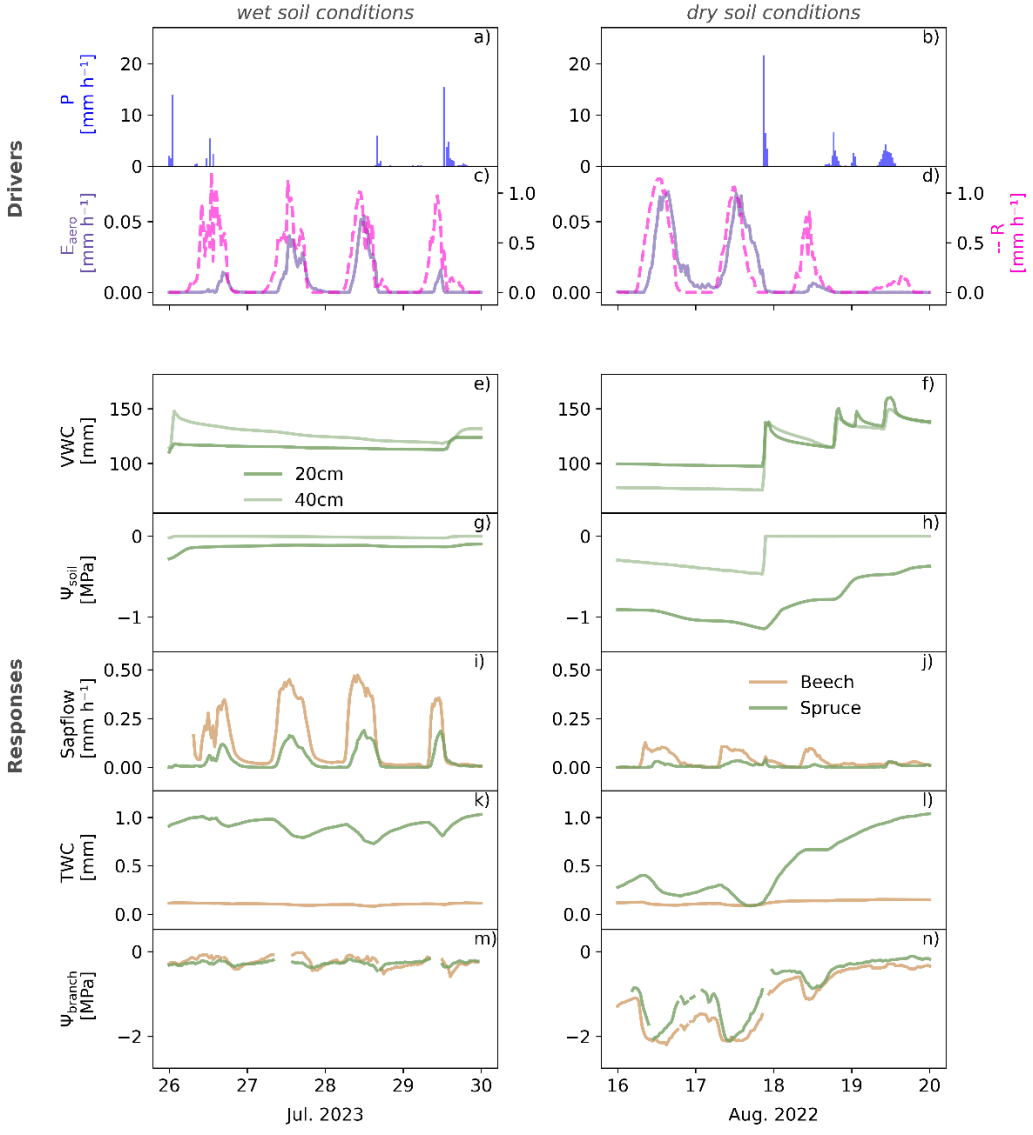

Figure 2: Half-hourly aggregates of measured impulse and response variables during four days of wet soil conditions (left column) and four days of dry soil conditions, shifting to wetter conditions (right column). The impulse variables are precipitation P (a&b), aerodynamic evaporative demand Eaero (solid lines, c&d), and solar radiation R (dashed lines, c&d). The response variables in the soil are volumetric water content VWC (e&f) and soil water potentials Ψsoil (g&h). The response variables in beech and spruce trees are sapflow (i&j), tree water content TWC (k&l) and branch water potential Ψbranch (m&n). For the sake of clarity, only the soil responses measured at 20 cm and 40 cm depth at the spruce cluster are shown, as soil responses look similar across depths and species (see impulse-response functions in Figs. 4&5, and Fig. C3 in Appendix C). The sapflow and tree water content responses are shown for one beech and one spruce tree. The branch water potential responses shown here were obtained by averaging data from all available psychrometers installed on beech branches, therefore represent a species-averaged branch water potential signal

https://doi.org/10.5194/egusphere-2026-2481
Preprint. Discussion started: 8 May 2026

measured at the site. The responses of beech and spruce trees, particularly of sapflow and branch water potential, highlight the strong reduction in sapflow and branch water potentials that occurs due to soil dryness. The transformed variables into units of mm h-1 are shown in Fig. S8, and the full measurement period is shown in Figures C2 to C7 in Appendix C.

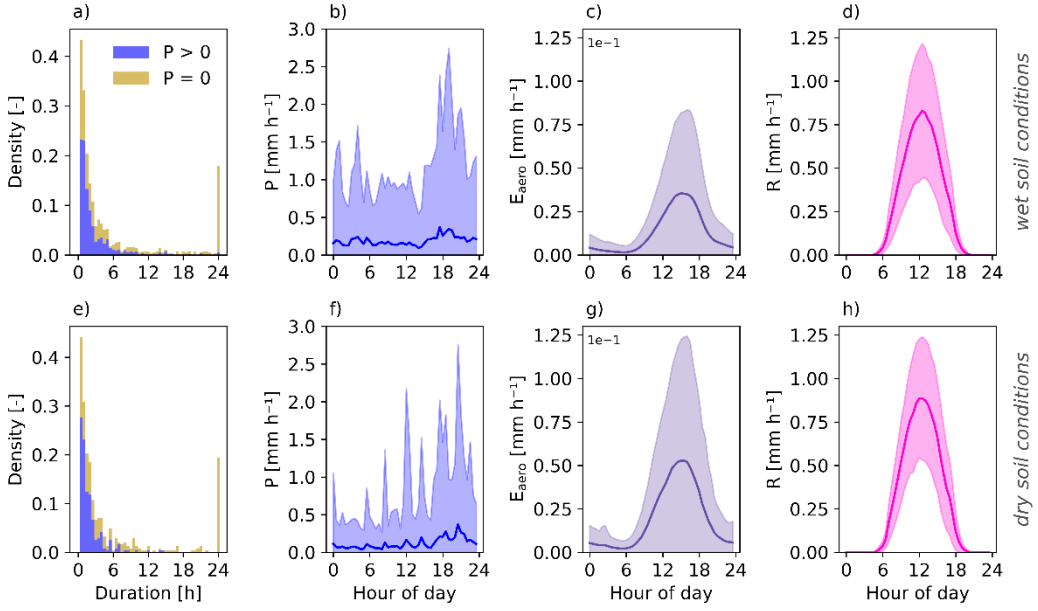

Figure 3: Durations of precipitation events (a&e) and diel patterns of precipitation (b&f), aerodynamic evaporative demand E_{aero} (c&g), and solar radiation R (d&h) during the growing season. Note that the 24-hour duration bar in panels a&e also includes dry events with a duration longer than 24 hours. Lines depict mean half-hourly measurements of diel precipitation (b&f), E_{aero} (c&g) and solar radiation R (d&h) dynamics. The shading around the mean indicates +/- one standard deviation of measurements at the specific half-hour of the day. The lower bound is truncated at 0 for precipitation (b&f) and E_{aero} (c&g).Top and bottom rows show measurements under wet (a-d) and dry (e-h) soil conditions (we define dry soil conditions as average soil water potentials of less than -0.5 MPa at 20 cm depth). E_{aero} increased under dry soil conditions, whereas precipitation patterns and radiation dynamics remained similar between wet and dry soil conditions.

3.2. Impulse-response functions of trees

3.2.1. Tree impulse response to precipitation

In the following, we present the impulse-response functions estimated by ERRA from ecosystem water fluxes and change of states. The left columns of Figs. 4 and 5 show the responses of beech and spruce, respectively, to impulses of precipitation. In both species, net tree water balance increases strongly, and rapidly, in response to precipitation (Figs. 4d, 5d). This response is faster in beech than in spruce, potentially reflecting the greater capacitance of tree water storage in spruce (Martinetti et al., 2026). Note that the response variable is the rate of change of tree water content; thus Fig. 4d shows that in beech, tree water content increases for less than one hour after precipitation under wet soil conditions, but about two hours under dry soil

https://doi.org/10.5194/egusphere-2026-2481
Preprint. Discussion started: 8 May 2026

conditions. Likewise, Fig. 5d shows that in spruce, tree water content increases about two hours after precipitation under wet soil conditions, but for more than 10 hours under dry soil conditions. The response is also stronger, in both species but more markedly in spruce, under dry soil conditions than under wet soil conditions, potentially reflecting the larger tree water deficits that occur during dry soil conditions, and the greater water storage capacity of spruce relative to beech. Net changes in branch water potential exhibit responses to precipitation (Figs. 4g, 5g) that are broadly similar to, but less distinct than, those of net tree water balance (Figs. 4d, 5d). Sapflow response to precipitation is indistinguishable from zero in beech (Fig. 4a), except for a negative response at lags around 2 hours and a positive response around 8 hours under dry soil conditions. In spruce (Fig. 5a), sapflow response to precipitation is weakly positive at short lags and indistinguishable from zero otherwise. The relatively indistinct responses of sapflow to precipitation suggest that although precipitation is an important control on water availability for tree water uptake, it is not an important driver of sapflow in the short term.

3.2.2. Tree impulse response to radiation and E_{aero}

Unlike precipitation, radiation and aerodynamic evaporative demand E_{aero} are dominant drivers of potential evapotranspiration, and thus can be expected to affect tree water fluxes. The middle and right columns of Figs. 4 and 5 show the impulse responses of beech and spruce to E_{aero} and radiation. Sapflow responds strongly to E_{aero} and radiation in both beech (Figs. 4b,c) and spruce (Figs. 5b,c), with a markedly longer-lasting response to radiation in spruce (Fig. 5c) than in beech (Fig. 4c), reflecting spruce's greater capacitance. In both species, sapflow response to radiation is similar in wet and dry soil conditions (Figs. 4c, 5c), but sapflow response to E_{aero} is more damped under dry soil conditions (Figs. 4b, 5b), plausibly reflecting the effects of soil dryness on stomatal conductance. In spruce, sapflow response to E_{aero} exhibits a marked transition from positive values at short lags to negative values at lags of 1-2 hours, potentially reflecting the lagged response of stomatal closure to changes in evaporative demand. This same transition from positive to negative in not observed in beech, potentially reflecting beech's weaker stomatal response to E_{aero} (i.e., less isohydric behavior) and spruce's greater capacitance (Ulrich and Grossiord, 2023; Martinetti et al., 2026).

Net tree water balance exhibits sharp, brief negative responses to E_{aero} and radiation in both beech (Fig. 4e,f) and spruce (Fig. 5e,f). Note that these are net rates of change in tree water content, and thus correspond to sharp step increases in tree water deficits. This step change is delayed by about 30 minutes in spruce but is nearly instantaneous in beech, reflecting the greater capacitance of spruce. Branch water potentials exhibit rapid negative responses to radiation in both species (Figs. 4i and 5i); again these are rates of change in Ψ_{branch} and thus represent sharp step decreases in branch water potentials. However the response of branch water potentials to E_{aero} is indistinct in both species (Figs. 4h and 5h), for reasons that remain unclear. From a physiological standpoint, stomata can be expected to open in response to increases in radiation ((all else equal; Shimazaki et al., 2007), consistent with the observed increases in sapflow and decreases in tree water content and branch water potential. There is no analogous physiological reason for stomata to open in response to increases in E_{aero}; on the contrary, they

https://doi.org/10.5194/egusphere-2026-2481
Preprint. Discussion started: 8 May 2026

can be expected to close when E_{aero} is high and water potentials are low. It nonetheless remains puzzling how the response of both species to E_{aero} can exhibit clear increases in sapflow and decreases in tree water content, without any identifiable change in branch water potentials.

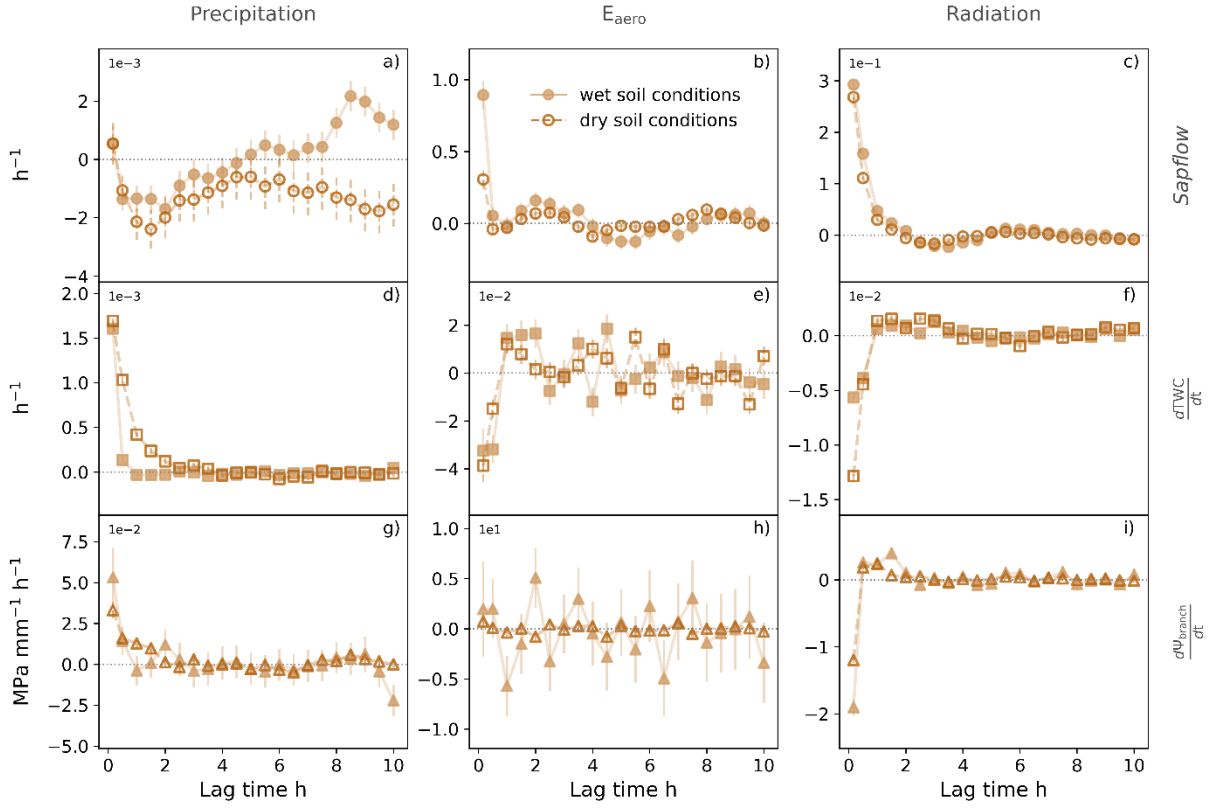

Figure 4: Beech trees - Impulse responses of sapflow (a-c), net tree water balance (dTWC/dt, d-f) and net change in branch water potential (dΨbranch/dt, g-i) to impulses of precipitation (left column), Eaero (middle column) and solar radiation (right column). Full and empty markers show mean responses under wet and dry soil conditions, respectively, as distinguished by a threshold of -0.5 MPa in average soil water potentials at 20 cm. This threshold roughly corresponds to the 0.3-quantile of the average soil water potential at 20 cm depth measured at the beech cluster. The whiskers show +/- one standard error of the mean. The impulse responses peak immediately and last only ~1 to 2 hours for all variables except sapflow, which exhibits a second peak in the response to precipitation after ~8 hours under wet soil conditions.

https://doi.org/10.5194/egusphere-2026-2481
Preprint. Discussion started: 8 May 2026

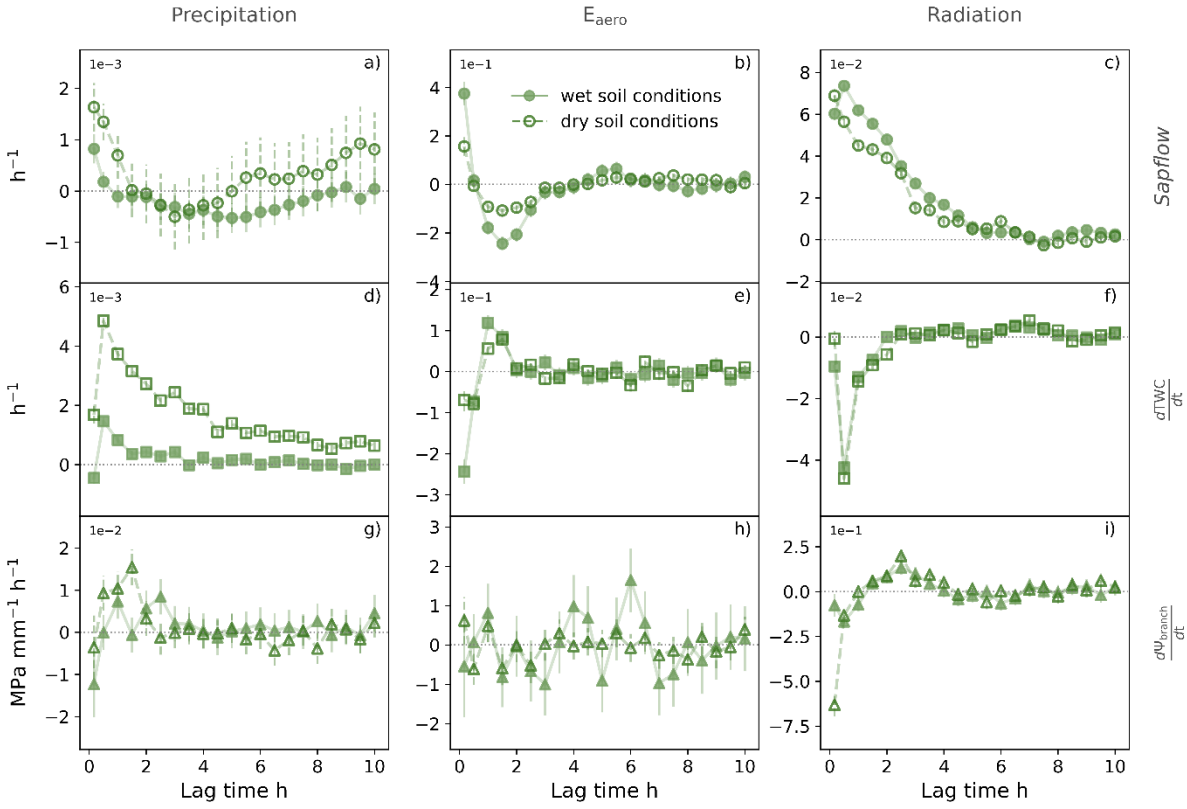

Figure 5: Spruce trees - Impulse response of sapflow (a-c), net tree water balance (dTWC/dt, d-f) and net change in branch water potential (dΨbranch/dt, g-i) to impulses of precipitation (left column), Eaero (middle column) and solar radiation (right column). Full and empty markers show mean responses under wet and dry soil conditions, respectively, as distinguished by a threshold of -0.5 MPa in average soil water potentials at 20 cm. This threshold roughly corresponds to the 0.16-quantile of the average soil water potential at 20 cm depth measured at the spruce cluster. Full markers show the mean impulse-response function under wet soil conditions, when average soil water potential at 20 cm was higher than -0.5 MPa. The whiskers show +/- one standard error of the mean. The responses peak in the first 3 hours in all variables (except where responses are indistinct, e.g., in panels g and h). Under dry soil conditions, the response of net tree water balance to precipitation is markedly stronger, as is the short-term response of branch water potential to radiation, whereas the response of sapflow to Eaero is more damped.

3.2.3. Hydraulic capacitance and stomatal regulation explain differences in impulse-response functions between beech and spruce

Relative to beech, spruce exhibited much lower sapflow rates than beech, but much larger variations in tree water content (Fig. 2i-l), reflecting spruce's greater hydraulic capacitance (and thus greater resilience against transient changes in soil water availability). While beech and spruce trees exhibit broadly similar responses to atmospheric controls, there are differences in the shape, magnitude, duration and timing of their impulse-response functions. The response of sapflow to solar radiation is smaller for spruce than for beech, but lasts significantly longer (Fig. 4c & 5c), illustrating how the greater capacitance of spruce

https://doi.org/10.5194/egusphere-2026-2481
Preprint. Discussion started: 8 May 2026

provides a more elastic buffer for tree water losses to transpiration, one that is re-filled more gradually by sapflow. The longer time to refill water storage in spruce can also be observed in the response of the net tree water balance to precipitation impulses, with spruce tree water content continuing to increase for more than 10 hours following precipitation impulses under dry soil conditions (Fig. 4d). By contrast, beech's less elastic tree water storage was typically refilled within the first 2 hours after precipitation impulses (Fig. 5d). Furthermore, peak responses of the net tree water balance occur within the same half hour as precipitation or radiation impulses in beech (Figs. 4d,f), but 30 minutes after precipitation or radiation impulses in spruce (Figs. 5d,f). This slower response of spruce trees likely reflects time needed to refill internal water storage in the roots (when precipitation impulses increase soil water availability) and to deplete internal water storage in the branches (when radiation impulses force transpiration). In other words, water storage of spruce tissues is first refilled or depleted near its source or sink, before the refill or depletion signal propagates to the point where tree water content is measured (i.e., at the tree stem at breast height). Similarly, branch water potentials of beech respond immediately to precipitation impulses (Fig. 4g), but due to the larger water storage capacity of spruce, the positive response in branch water potential occurs ~1 hour later, lasts longer, and is less distinct (Fig. 5g).

The immediate response of net tree water balance to radiation impulses is roughly twice as strong under dry soil conditions than under wet soil conditions in beech (Fig. 4f), but is similar between wet and dry soil conditions in spruce (Fig. 5f). By contrast, the immediate response of net tree water balance to E_{aero} is half as large under dry soil conditions than under wet soil conditions in spruce (Fig. 5e), but is similar between wet and dry soil conditions in beech (Fig. 4e). This suggests that stomatal responses to E_{aero} are more sensitive to soil moisture in spruce than in beech, consistent with the characterization of spruce as being more isohydric than beech (Hesse et al., 2022; Knüver et al., 2022; Martinetti et al., 2025). In spruce, the responses of sapflow and tree water balance to E_{aero} (Fig. 5b,e) exhibit damped oscillations, changing sign before stabilizing near zero, consistent with lags in the negative feedbacks underlying stomatal regulation. Similar damped oscillations may also be present in beech (Fig. 4b,e), but are less distinct. The mechanisms controlling stomatal closure are more likely to be passive for spruce (a gymnosperm) and active for beech (an angiosperm). Passive closure is regulated by hydraulics and guard cell movement following changes in turgor water pressure (e.g., Brodribb and McAdam, 2017) and active closure is affected by abscisic acid signalling (e.g., McAdam and Brodribb, 2014). The more distinct oscillations in spruce might reflect a lagged negative feedback of stomatal regulation, related to the required hydraulic equilibration times of stomatal guard cells in passive stomatal control.

3.3. Impulse-response functions in the soil

For the sake of clarity, here we only show impulse-response functions of soil water dynamics at 20 cm depth, with similar results at 10 cm, 40 cm and 80 cm shown in Fig. C9-C14 in Appendix C. Because the patterns of response are mostly similar between the beech and spruce clusters, the comments below apply to both unless otherwise noted.

https://doi.org/10.5194/egusphere-2026-2481
Preprint. Discussion started: 8 May 2026

Under dry soil conditions, net soil water recharge and net changes in soil water potentials respond quickly to precipitation (Figs. 6a,b and 7a,b); because analyzed variables are derivatives, these spikes correspond to step increases in volumetric water content and soil water potentials. Under wet soil conditions, the response of net soil water recharge is reduced, and the response of soil water potential is not detectable (presumably because water potentials are already close to zero).

On daily time scales, the peak response of soil water recharge to precipitation occurs on the same day that rain falls if soil conditions are wet (filled symbols, Figs. 6g and 7g), but if soil conditions are dry, the peak response of soil water recharge and soil water potential occurs on the day after rain falls (open symbols, Figs. 6g,j and 7g,j). This seems counterintuitive in view of the fast response seen in the half-hourly data, but it arises from the two different aggregation time scales (30 minutes vs 24 hours), together with the fact that we are measuring the impulse response in the derivatives, and the fact that intense precipitation tends to fall late in the day (see Fig. 3). Figure C15 in Appendix C illustrates the phenomenon using a simple example of a pulse input of precipitation falling at 18:00, which generates a step increase in VWC that persists for several days, consistent with the quick spike response in the derivative of VWC, as shown in Figs. 6a and 7a. This step increase will be diluted by a factor of 4 when it is averaged over the day that the rain fell (because it occurred only in the last 6 hours of the day), but no similar dilution will occur in the following day. Thus when we take derivatives based on daily averages the increase in VWC on the day the rain falls will appear smaller than the increase on the day after the rain falls.

A comparison between beech and spruce soils reveals that responses in soil water content are stronger below spruce trees than below beech trees, potentially because of the increased interception capacity of beech canopies during the main growing season. The sharp spike in soil water recharge at 20 cm depth is followed by a small, brief period of negative net recharge at a lag of about 0.5-1 hour (Figs. 6a, 7a). This may reflect the propagation of the wetting front to deeper layers, as observed by Gao et al. (in press). Dry soil conditions trigger stronger responses, particularly at soil depths of 20 cm (Figs. 6&7) and 40 cm (Fig. C10 & C13 in Appendix C); by contrast, under wet soil conditions, there is less capacity for retaining net soil water recharge, because water potentials are already close to 0.

One might expect that impulses in E_{aero} or solar radiation, both forcing transpiration, would lead to decreases in soil water contents. However, the calculated responses fluctuate around 0 for time lags of up to 10 hours (Figs. 6b,c,e,f and 7b,c,e,f), particularly under dry soil conditions. By contrast, the daily averages show clear negative responses of VWC to radiation impulses under both wet and dry soil conditions (Figs. 6i and 7i), and a negative responses of soil water potentials under dry soil conditions (Figs. 6l and 7l). These observations plausibly reflect the time-integrated effects of root water uptake (resulting from radiation-driven transpiration) on soil moisture and soil water potentials over daily time scales. The same effects are indistinct on shorter time scales due to the buffering effects of water storage changes in the trees. Daily responses of soil

https://doi.org/10.5194/egusphere-2026-2481
Preprint. Discussion started: 8 May 2026

moisture and soil water potentials to E_{aero} are not distinctly observable (Figs. 6h,k and 7h,k), potentially due to the trees' stomatal response to changes in E_{aero}.

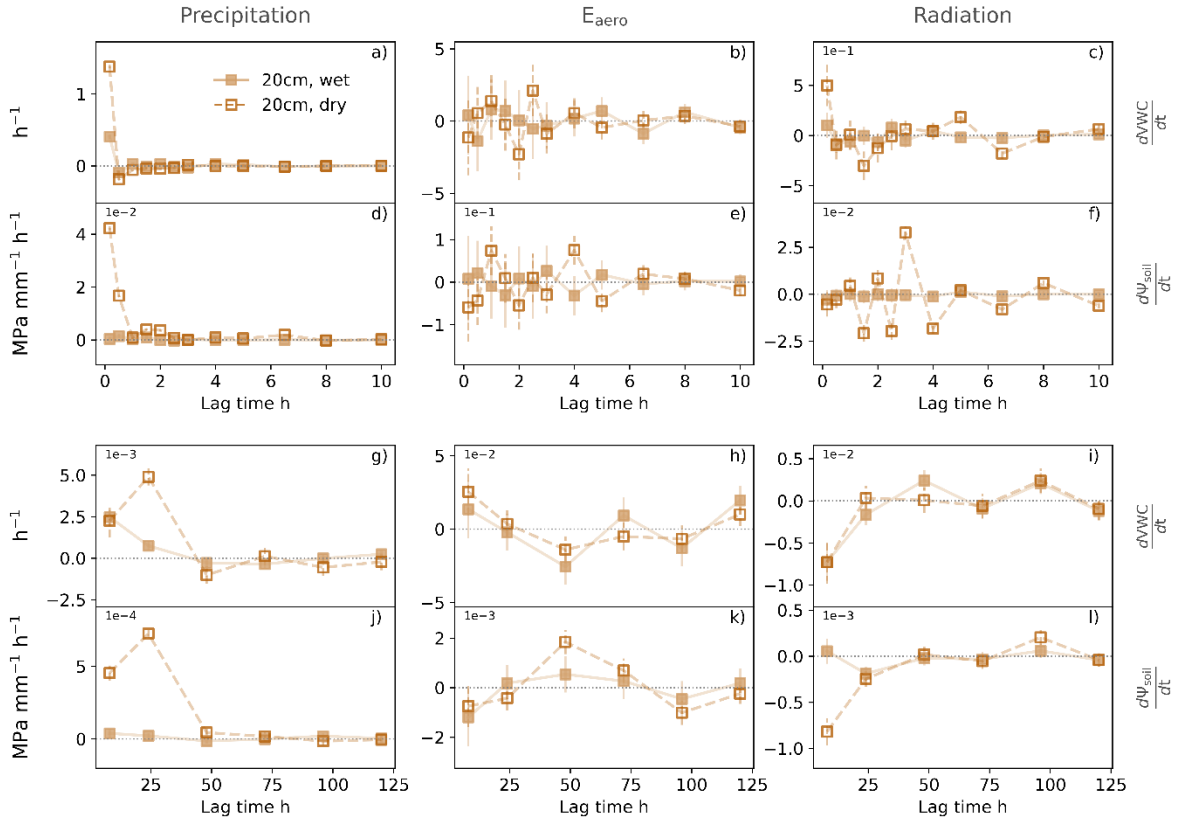

Figure 6: Beech soil cluster - Impulse responses of net soil water recharge (dVWC/dt) and net change in soil water potential (dΨsoil/dt) to impulses of precipitation (left column), Eaero (middle column) and solar radiation (right column), for 20 cm depth within the beech cluster. The upper two rows (a-f) show short-term (0-10 hour) impulse-response functions of half-hourly data, while the lower two rows (g-l) show impulse-response functions over 0-5 days. Full and empty markers show mean responses under wet and dry soil conditions, respectively, as distinguished by a threshold of -0.5 MPa in average soil water potentials at 20 cm. This threshold roughly corresponds to the 0.3-quantile of the average soil water potential at 20 cm depth measured at the beech cluster. The whiskers show +/- one standard error of the mean. Short-term responses to precipitation peak immediately, and are stronger during dry soil conditions. The short-term responses to Eaero and solar radiation are highly uncertain in the first ~5 hours. Daily responses to radiation show soil water depletion (negative net soil water recharge), as well as decreases in soil water potentials under dry soil conditions.

https://doi.org/10.5194/egusphere-2026-2481
Preprint. Discussion started: 8 May 2026

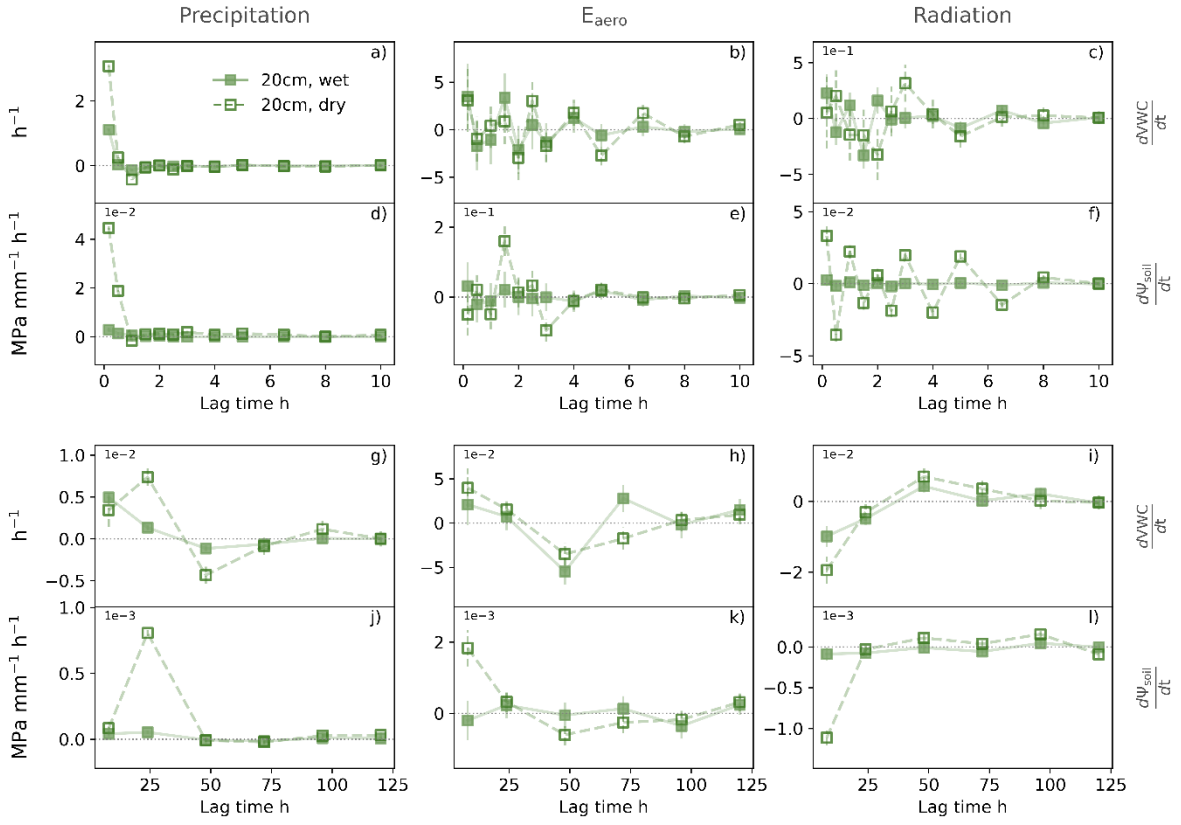

Figure 7: Spruce soil cluster - Impulse responses of net soil water recharge (dVWC/dt) and net change in soil water potential (dΨsoil/dt) to impulses of precipitation (left column), Eaero (middle column) and solar radiation (right column), for 20 cm depth within the spruce cluster. The upper two rows (a-f) show short-term (0-10 hour) impulse-response functions of half-hourly data, while the lower two rows (g-l) show impulse-response functions over 0-5 days. Full and empty markers show mean responses under wet and dry soil conditions, respectively, as distinguished by a threshold of -0.5 MPa in average soil water potentials at 20 cm. This threshold roughly corresponds to the 0.16-quantile of the average soil water potential at 20 cm depth measured at the spruce cluster. The whiskers show +/- one standard error of the mean. Short-term responses to precipitation peak immediately, and are stronger during dry soil conditions. The short-term responses to Eaero and solar radiation are highly uncertain in the first ~5 hours. Daily responses to radiation show soil water depletion (negative net soil water recharge), as well as decreases in soil water potentials under dry soil conditions.

4. Summary and outlook

We applied ERRA to water fluxes and changes in water states within the soil-plant-atmosphere continuum of a mixed beech-spruce forest. The resulting impulse-response functions reveal species-specific functional traits influencing tree-mediated water fluxes driven by precipitation, aerodynamic evaporative demand (E_{aero}) and solar radiation. The impulse-response functions were obtained directly from field data, without process modeling assumptions. Our results offer a data-driven alternative to other methods for assessing ecosystem functioning, including controlled experiments (Gebhardt et al., 2023;

https://doi.org/10.5194/egusphere-2026-2481
Preprint. Discussion started: 8 May 2026

Hesse et al., 2022; Huxman et al., 2004b; Knüver et al., 2022; Piayda et al., 2017; Werner et al., 2021), model simulations (Collins et al., 2014; Grant et al., 2012; Paschalis et al., 2015) complex statistical approaches where underlying assumptions are sometimes violated (e.g., temporal independence of measurements; Chen *et al.*, 2026b) or black-box machine learning approaches (Bai et al., 2026; Chen et al., 2026a; Cranko Page et al., 2023; Qi et al., 2025). Our analysis illustrates how impulse-response functions can help in characterizing ecosystem functioning and understanding its system dynamics.

4.1. Beech and spruce trees show fast responses and differing internal storage effects

Precipitation impulses led to rapid increases in water contents and water potentials after precipitation events. Similarly to (Ma et al., 2025), we found stronger responses in tree and soil water contents to precipitation falling under drier antecedent soil conditions ($\Psi_{20\,cm}$ < -0.5 MPa), suggesting that soil water availability is an important control on tree-mediated water fluxes, modulating the response to atmospheric forcing (Kannenberg et al., 2019) across different ecosystems and within individual ecosystems. While sapflow response to radiation was similar between wet and dry soil conditions, sapflow response to E_{aero} was weaker under dry soil conditions, indicating that the trees regulated transpiration in response to impulses of E_{aero} (but not radiation) more strongly as soil water availability declined (Bai et al., 2026). Thus, dry soil conditions potentially reduce the light utilization efficiency of trees as a consequence of stomatal closure resulting from rising E_{aero} or vapor pressure deficit (Roby et al., 2020). Similarly, recent studies showed how ecosystem light utilization efficiency was increasingly determined by VPD in drier soils (Fu et al., 2025) or coarser soils (Wankmüller et al., 2024), both of which reduce soil water availability for plants. By contrast, tree water fluxes and carbon uptake are less stringently regulated by stomatal closure when soil water availability is high. Such conditions typically occur after precipitation events and lead to recovery in transpiration rates as a consequence of stomatal opening and increased photosynthetic rates (Huxman et al., 2004a, b; Wang et al., 2015).

Our results indicate that following precipitation impulses, tree water storage rapidly rises, either through enhanced tree water uptake or decreased transpiration (due to canopy wetting inhibiting transpiration from the leaves, which would not be reflected in E_{aero} as inferred from weather station measurements outside the canopy). However, previous isotope studies have shown that most xylem water in similar ecosystems (Allen et al., 2019), and at our site specifically (Floriancic et al., 2024) originates from winter-season precipitation. These isotope studies seemingly contradict the rapid water uptake after summer precipitation events. A potential resolution of this apparent paradox could be that, when soils become dry (and thus the characteristic curve relating soil water potential and soil water content becomes steep), small additions of precipitation can make the water that is already stored in soils available to trees by enhancing the water potential in the soil. The mixing time of new precipitation water with water already contained in soils has been shown to take several hours (Liu et al., 2026), spanning a similar duration as the response in water uptake by our estimated impulse-response functions.

https://doi.org/10.5194/egusphere-2026-2481
Preprint. Discussion started: 8 May 2026

4.2. Trees buffer and shield soil from the atmosphere

Figures 4 and 5 show that trees at our study site respond quickly and strongly to atmospheric forcing by E_{aero} and radiation, whereas Figs. 6 and 7 show no systematic soil responses to short-term E_{aero} and radiation forcing. This observation leads to the obvious question: why do the trees exhibit such clear responses, and the soils don't? Trees are strongly coupled to radiation forcing because the canopy intercepts most of the incident sunlight. But for the same reason, radiation forcing at the forest floor will be only a small fraction of that at the top of the canopy. Trees are also strongly coupled to E_{aero} because their canopies are directly exposed to the turbulent flow of the free atmosphere, and because the exposed canopy surface area is much larger than the underlying land surface (i.e., LAI is much greater than 1). The aerodynamic drag of the canopy strongly reduces below-canopy wind speeds, and thus strongly inhibits turbulent mixing between the forest floor and the free atmosphere. Evapotranspiration from the canopy and forest floor also makes humidity markedly higher below the canopy than above it. Canopy shading reduces temperatures at the forest floor, and thus reduces the vapor pressure deficit for any given level of absolute humidity. Thus by reducing wind speeds, raising humidity, and lowering ambient temperatures, the canopy greatly reduces E_{aero} below the canopy relative to E_{aero} above the canopy. Because radiation forcing and E_{aero} are greatly reduced at the forest floor relative to the top of the canopy, the variability of radiation forcing and E_{aero} at the soil surface is small compared to that which is experienced by the trees (or is measured by the weather station). The forest-floor litter layer further insulates the underlying soils from atmospheric forcing. Because the forcing by E_{aero} and radiation at the soil surface is weak, the response of the soils to that forcing is weak and indistinct (Figs. 6b,c,e,f and 7b,c,e,f).

On daily timescales, however, one can detect responses to radiation forcing in both soil water content and soil water potential (Figs. 6i,l and 7i,l), suggesting that the strong responses of the trees to radiation forcing (Figs 4c,f,i and 5c,f,i) are being transmitted to the soil via root water uptake. Any such transmission will be buffered on short timescales by capacitance within the tree. We see no clear evidence suggesting transmission of E_{aero} responses through root water uptake on daily timescales, possibly because E_{aero} effects are more likely to be compensated by stomatal closure than radiation effects are.

Figures 6a,d and 7a,d show that soils respond quickly and strongly to precipitation forcing, whereas Figs. 4a and 5a show only a relatively weak response of sapflow to precipitation. This observation suggests that, just as the forest canopy buffers and shields the soil from impulses of E_{aero} and radiation, the soil seems to buffer sapflow from precipitation forcing. Tree water content, however, responded rapidly to precipitation (Figs. 4d and 5d). Rapid responses in tree water content without corresponding responses in sapflow suggest that tree water content increases after precipitation events are primarily due to decreased transpiration (due to canopy wetting), rather than to rapid replenishment of tree water content as soil water availability increases. By contrast, sapflow exhibited distinct responses to solar radiation (Figs. 4c and 5c) that lasted longer in spruce trees than in beech trees, consistent with larger hydraulic capacitance of spruce than beech (Martinetti et al., 2026). The longer-lasting responses of sapflow to radiation in spruce trees presumably reflects refill of tree water storage above the

https://doi.org/10.5194/egusphere-2026-2481
Preprint. Discussion started: 8 May 2026

sapflow sensor. We do not observe an equivalent sapflow response to precipitation, despite rapid increases in soil moisture (under both wet and dry soil conditions; Figs 6a and 7a) and sharp increases in soil water potentials (under dry, but not wet, soil conditions; Figs. 6d and 7d). The weak sapflow response to precipitation may imply that soil water availability to the trees does not improve as much as one might think (because soil water potentials rise only in dry soils, which prevail only 16-30% of the time). Alternatively, it may imply that rising soil water availability does not lead to rapid replenishment of tree water above-ground, either because precipitation depresses evaporative demand by wetting the canopy, or because subsurface (i.e., root) water storages are replenished first, once soil water availability rises.

4.3. Limitations and outlook

We analyzed time series of ecosystem water fluxes, storages, and potentials in soils and trees. For some variables (soil matric potential at 20 cm depth and tree water fluxes and states) we installed several sensors in multiple locations or multiple trees. However, sensors at specific locations in the soil or on specific tree segments capture ecosystem water fluxes only at those points (i.e., stem measurement at breast height for sapflow and tree water content). The impulse-response functions showed differences in timing and duration of impulse responses in beech and spruce, likely originating from differences in hydraulic capacitance and stomatal regulation between the two species. However, we lack accurate measurements of transpiration rates because sapflow measurements were strongly affected by tree water storage dynamics on the time scales analyzed here. Accurate transpiration measurements, for example obtained with eddy covariance flux towers, could be used to infer impulse-response functions reflecting stomatal regulation dynamics of beech and spruce more directly. Furthermore, we considered E_{aero} measured at the weather station outside the forest as a proxy for the aerodynamic evaporative demand. Although this is common practice in ecosystem water flux studies, the resistance to water movement from the leaves to the atmosphere is strongly determined by the depth of the turbulent boundary layer, which is controlled by humidity and wind speed at the canopy. Additionally, temperature affects stomatal conductance and transpiration by controlling photosynthetic capacity (Berry and Bjorkman, 1980; Wang et al., 2026), but in order to limit the complexity of our analysis, we did not include temperature as a forcing variable. Despite these limitations, our analysis shows how ERRA can be applied to ecosystem water fluxes and states to advance our understanding of ecosystem functioning. We therefore encourage its application on further datasets, potentially including eddy-covariance flux measurements, direct stomatal conductance measurements or more extensive soil water measurements.

https://doi.org/10.5194/egusphere-2026-2481
Preprint. Discussion started: 8 May 2026

Appendices

Appendix A: Tree properties

Table A1: Characteristics of trees at the WaldLab field site used for the study. The location of the trees is shown in Figure 1.

Tree	DBH [cm]	Sapwood depth [mm]	Sapwood area [cm^2]	Crown area [m^2]	Height [m]
Beech 2	33.5	63	537	29	16
Beech 3	24	31	243	17	18
Beech 4	34	40	372	29	17
Spruce 1	51	53	754	29	25
Spruce 2	21	42	224	7	21
Spruce 4	28	44	321	12	22
Spruce 5	34	43	389	15	23
Spruce 6	12	27	80	5	10

Appendix B: Granier type equation to convert temperature differences to sapflow densities

$$u = 213.625 * (\frac{dT_{max}}{dT_{actual}} - 1)^{1.509} \quad \text{(B1)}$$

where is u the sapflow density in $cm^3\ m^{-2}\ s^{-1}$, dT_{max} is the temperature difference occurring under zero-flow conditions (at predawn), calculated for a moving window of 5 days, and dT_{actual} is the current temperature difference.

https://doi.org/10.5194/egusphere-2026-2481
Preprint. Discussion started: 8 May 2026

Appendix C: Supplementary Figures

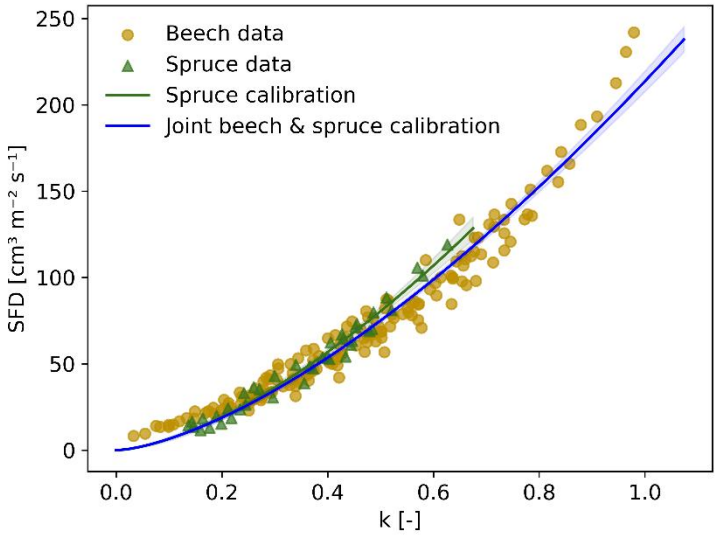

Figure C1: Calibration function (Eq. B1) used to convert temperature difference measured with sapflow sensors into sapflow densities. The red and green dots show data from Peters et al. (2021) for beech and spruce trees, respectively. The blue curve shows the joint calibration for beech and spruce data together, while the green curve shows the calibration for spruce data only. The shading around the curves show the 95% confidence of the fitted parameters. There is no substantial difference between the two species, which is why we used the same joint calibration for both species.

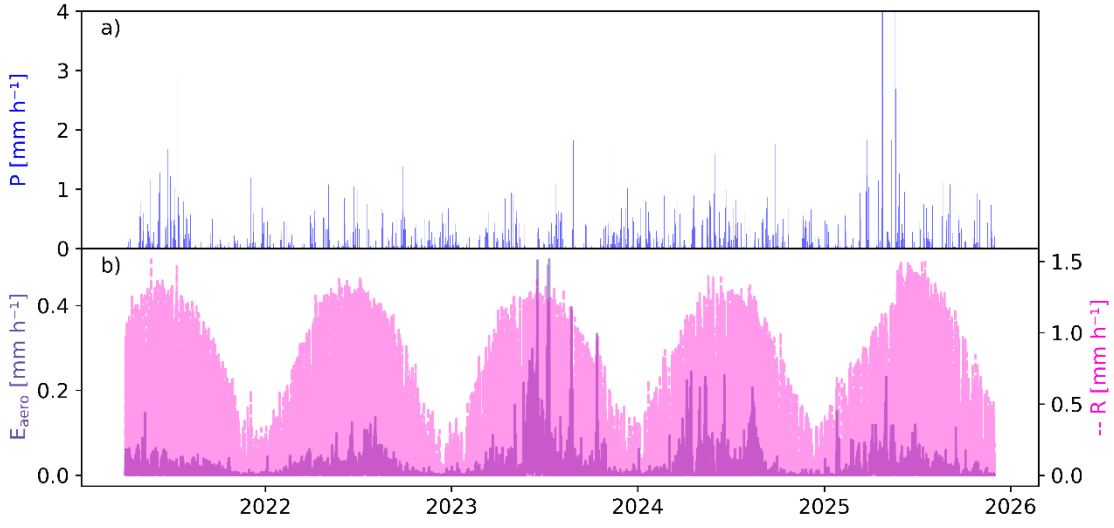

https://doi.org/10.5194/egusphere-2026-2481
Preprint. Discussion started: 8 May 2026

Figure C2: Precipitation (P; panel a), aerodynamic evaporative demand (E_{aero}; panel b) and solar radiation (R; dashed line in panel b) measured during the study period at the meteostation located approximately 150 from the study site outside the forest (see Fig. 1).

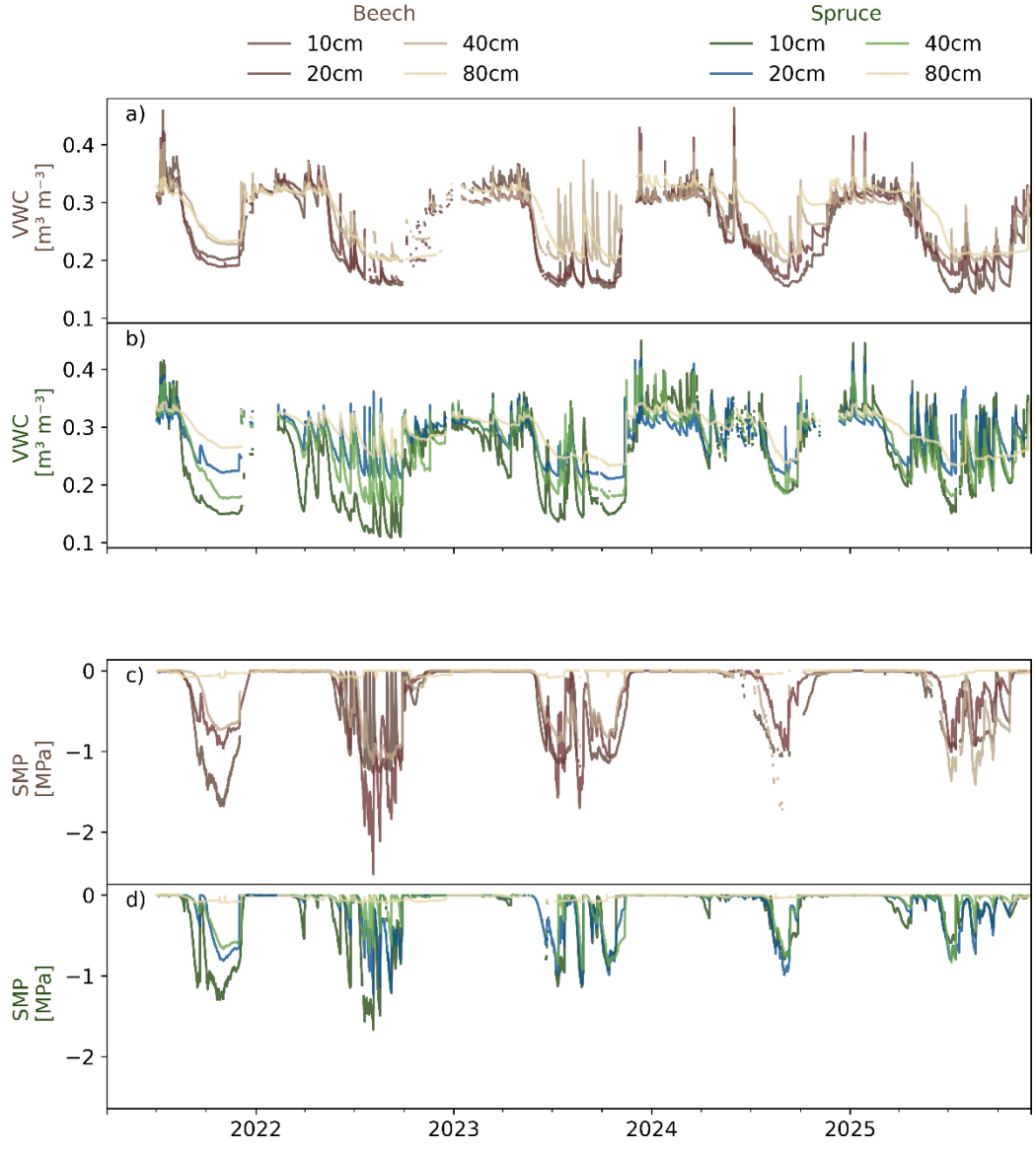

Figure C3: Soil measurements at the beech (a&c) and spruce (b&d) cluster at the study site during the study period (July 2021 to December 2025; see Fig. 1 for exact locations of the measurements) at 10cm, 20cm, 40cm and 80cm depth. Volumetric water content (VWC; a&b) was measured with Teros11 and Teros12 sensors. Soil water potential (Ψ_{soil}; c&d) was measured with Teros21 sensors at 10cm, 20cm and 40cm depth, and with Teros32 sensors at 80cm depth. Soil water potential at 20cm depth represents the average of multiple sensors and indicates lower water potentials in soils below the beech cluster compared to soils below the spruce cluster.

https://doi.org/10.5194/egusphere-2026-2481
Preprint. Discussion started: 8 May 2026

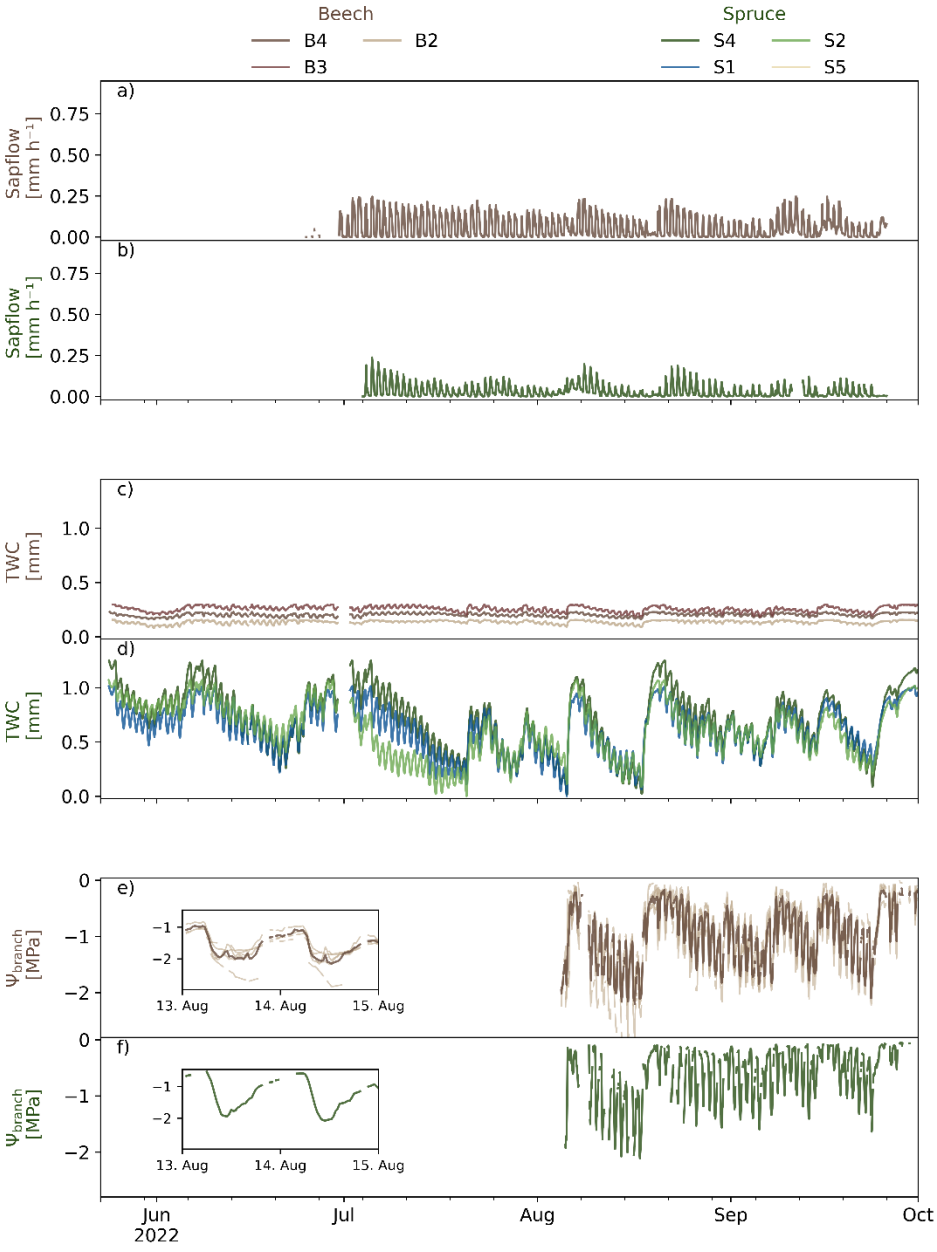

555 **Figure C4: Sapflow (a&b), tree water content (TWC; c&d) and branch water potential (Ψ_{branch}; e&f) measurements on beech (a,c,e) and spruce trees (b,d,f) at the study site (see Fig. 1 for the locations of the trees) during the growing season 2022. Branch water potentials measured with multiple psychrometers on beech trees (light brown) were averaged for Fig. 2.**

https://doi.org/10.5194/egusphere-2026-2481
Preprint. Discussion started: 8 May 2026

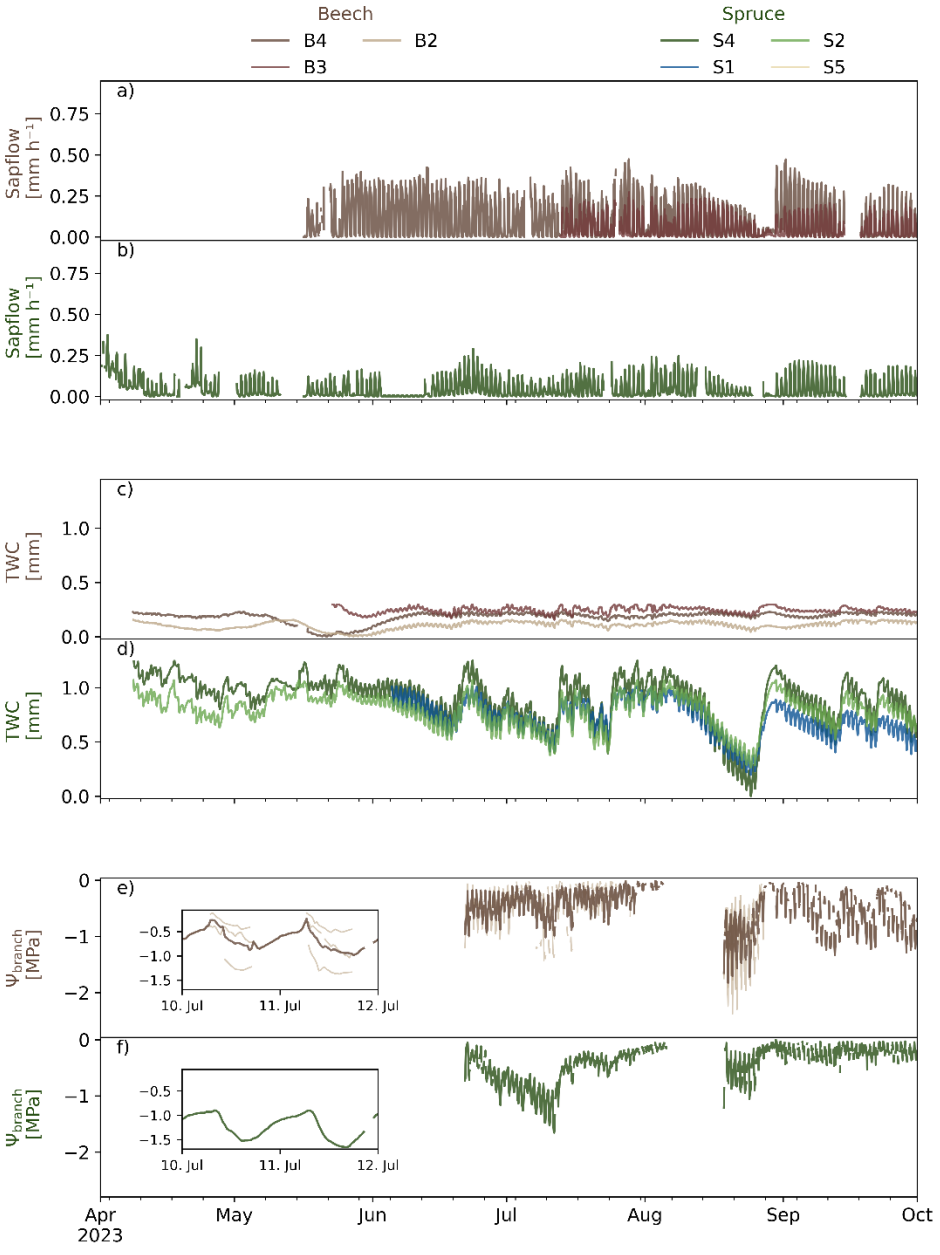

560 **Figure C5: Sapflow (a&b), tree water content (TWC; c&d) and branch water potential (Ψ_{branch}; e&f) measurements on beech (a,c,e) and spruce trees (b,d,f) at the study site (see Fig. 1 for the locations of the trees) during the growing season 2023. Branch water potentials measured with multiple psychrometers on beech trees (light brown) were averaged for Fig. 2.**

https://doi.org/10.5194/egusphere-2026-2481
Preprint. Discussion started: 8 May 2026

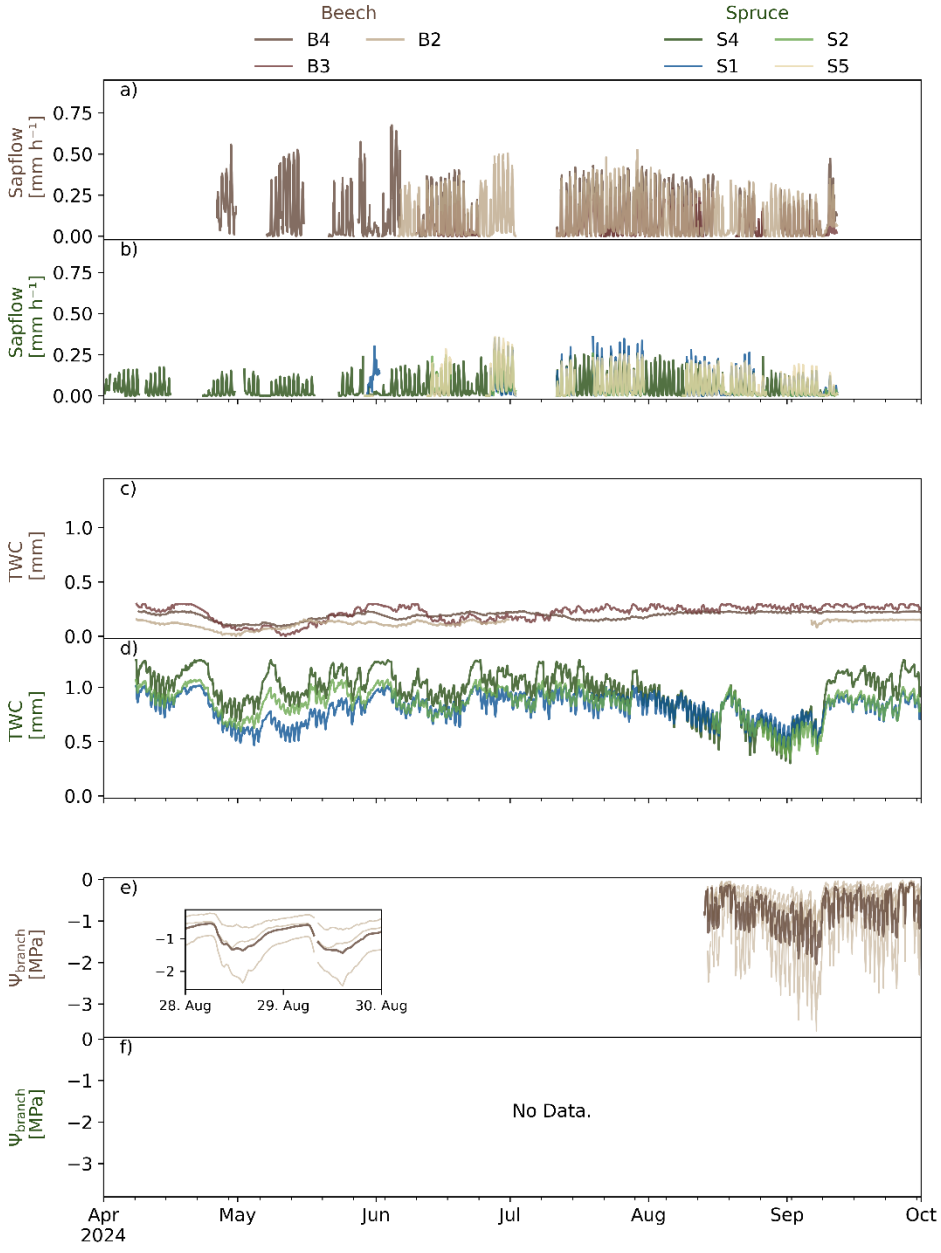

Figure C6: Sapflow (a&b), tree water content (TWC; c&d) and branch water potential (Ψ_{branch}; e&f) measurements on beech (a,c,e) and spruce trees (b,d,f) at the study site (see Fig. 1 for the locations of the trees) during the growing season 2024. Branch water potentials measured with multiple psychrometers on beech trees (light brown) were averaged for Fig. 2. No psychrometer were installed on spruce trees in 2024.

https://doi.org/10.5194/egusphere-2026-2481
Preprint. Discussion started: 8 May 2026

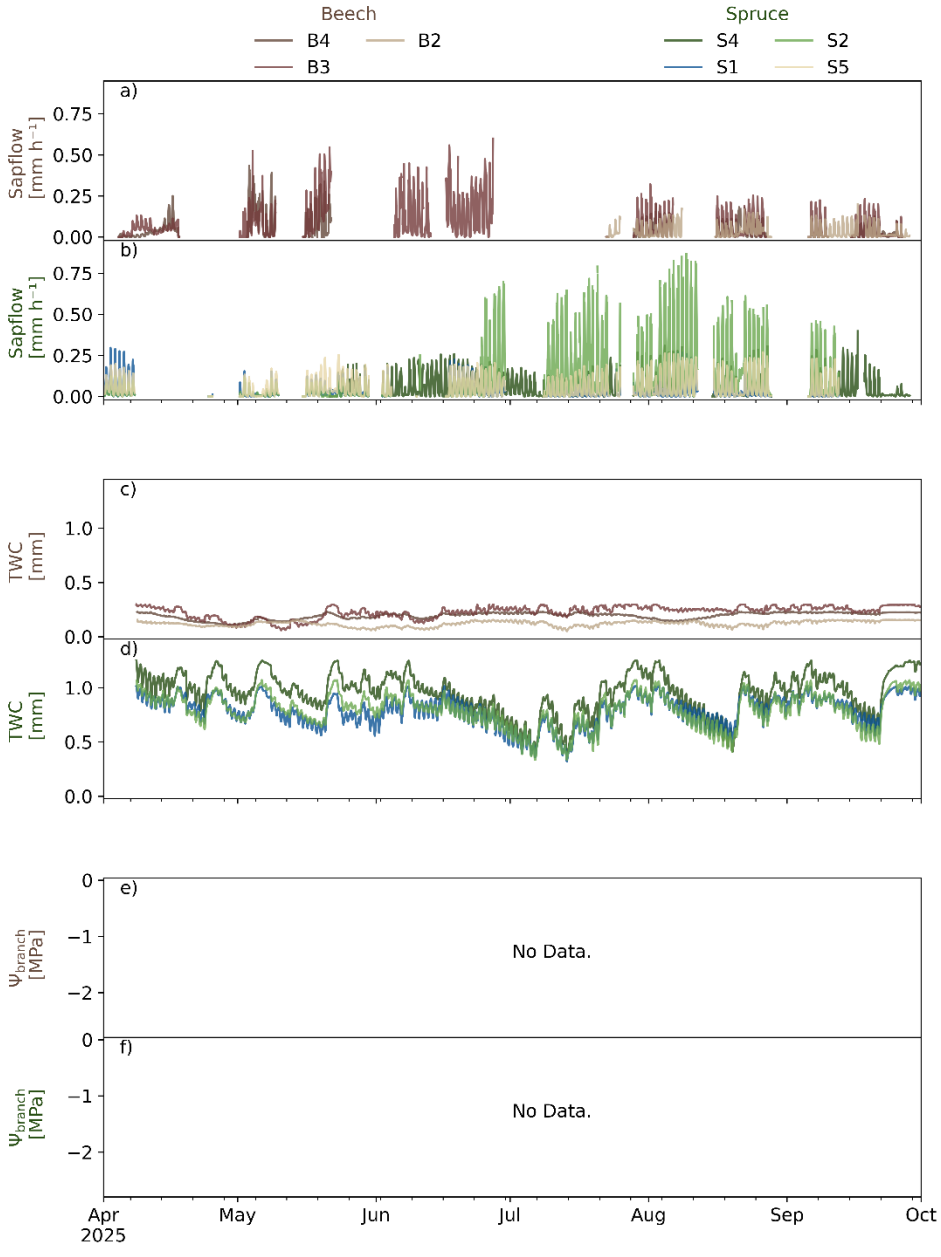

Figure C7: Sapflow (a&b), tree water content (TWC; c&d) and branch water potential (Ψ_{branch}; e&f) measurements on beech (a,c,e) and spruce trees (b,d,f) at the study site (see Fig. 1 for the locations of the trees) during the growing season 2025. No psychrometer were installed on beech or spruce trees in 2025.

https://doi.org/10.5194/egusphere-2026-2481
Preprint. Discussion started: 8 May 2026

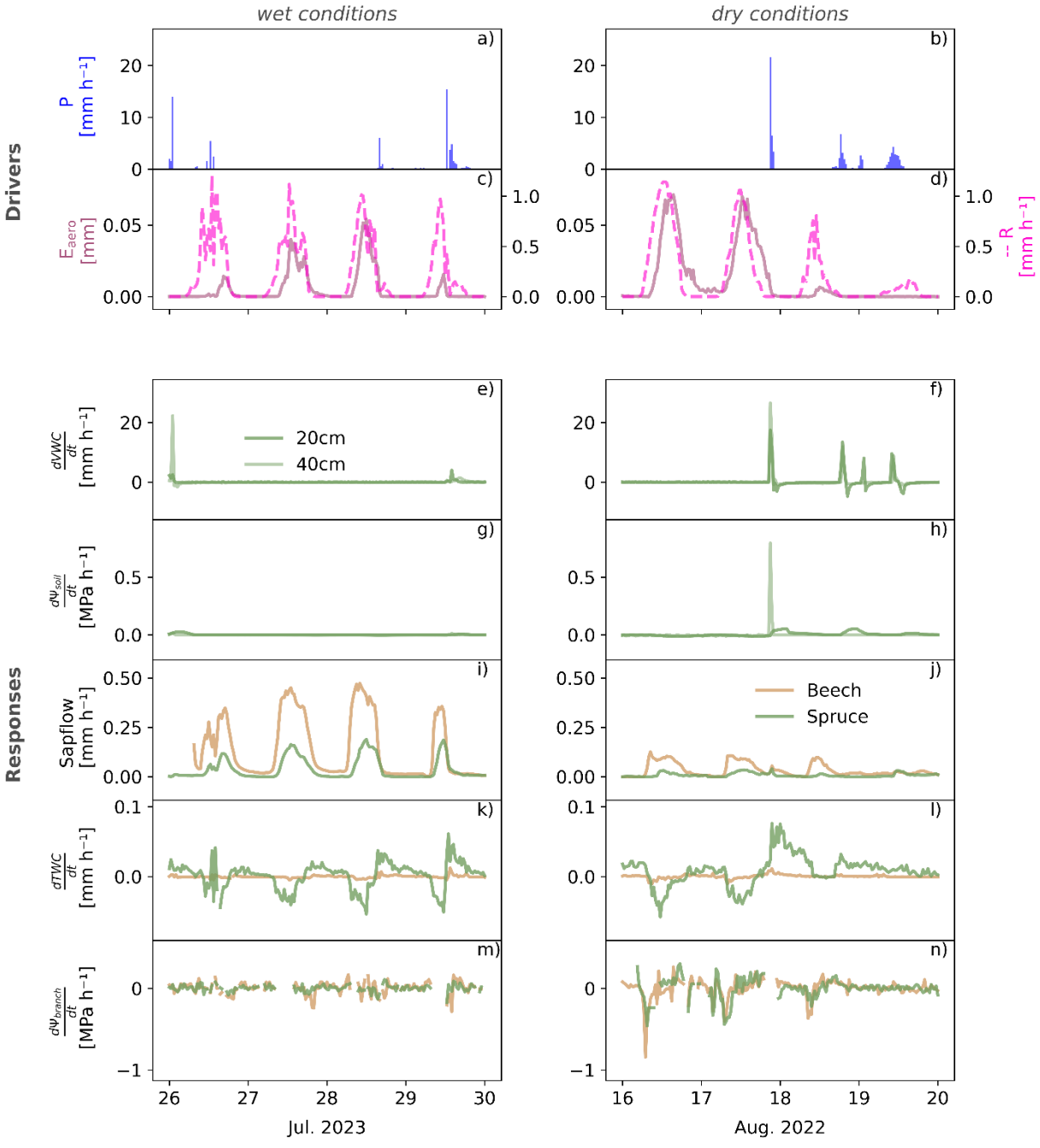

Figure C8: Half-hourly aggregates of measured impulse and response variables during four days of wet soil conditions (left column) and four days of dry soil conditions, shifting to wetter conditions (right column). The impulse variables are precipitation P (a&b),

https://doi.org/10.5194/egusphere-2026-2481
Preprint. Discussion started: 8 May 2026

aerodynamic evaporative demand Eaero (solid lines, c&d), and solar radiation R (dashed lines, c&d). The response variables in the soil are time derivatives volumetric water content (dVWC/dt - e&f) and soil water potentials (dΨsoil/dt - g&h). The response variables in beech and spruce trees are sapflow (i&j), time derivatives in tree water content (dTWC/dt - k&l) and branch water potential (dΨbranch/dt - m&n). For the sake of clarity, only the soil responses measured at 20 cm and 40 cm depth at the spruce cluster are shown, as soil responses look similar across depths and species. The sapflow and tree water content responses are shown for one beech and one spruce tree. The branch water potential responses shown here were obtained by averaging data from all available psychrometers installed on beech branches, therefore represent a species-averaged branch water potential signal measured at the site.

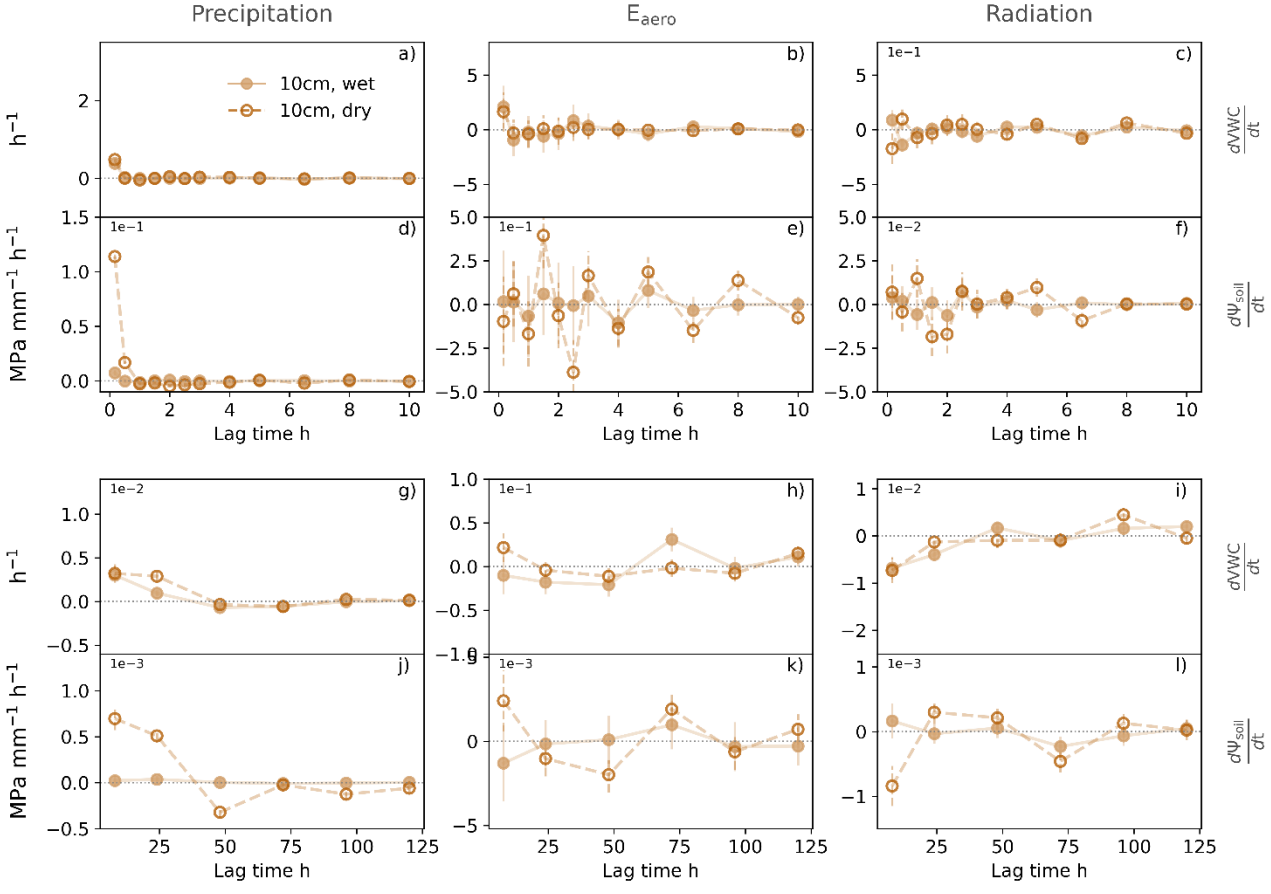

Figure C9: Beech soil cluster - Impulse responses of net soil water recharge (dVWC/dt) and net change in soil water potential (dΨsoil/dt) to impulses of precipitation (left column), Eaero (middle column) and solar radiation (right column), for 10 cm depth within the beech cluster. The upper two rows (a-f) show short-term (0-10 hour) impulse-response functions of half-hourly data, while the lower two rows (g-l) show impulse-response functions over 0-5 days. Full and empty markers show mean responses under wet and dry soil conditions, respectively, as distinguished by a threshold of -0.5 MPa in average soil water potentials at 20 cm. This threshold roughly corresponds to the 0.3-quantile of the average soil water potential at 20 cm depth measured at the beech cluster. The whiskers show +/- one standard error of the mean. Short-term responses to precipitation peak immediately, and are stronger during dry soil conditions. The short-term responses to Eaero and solar radiation are highly uncertain in the first ~5 hours. Daily

https://doi.org/10.5194/egusphere-2026-2481
Preprint. Discussion started: 8 May 2026

responses to radiation show soil water depletion (negative net soil water recharge), as well as decreases in soil water potentials under dry soil conditions.

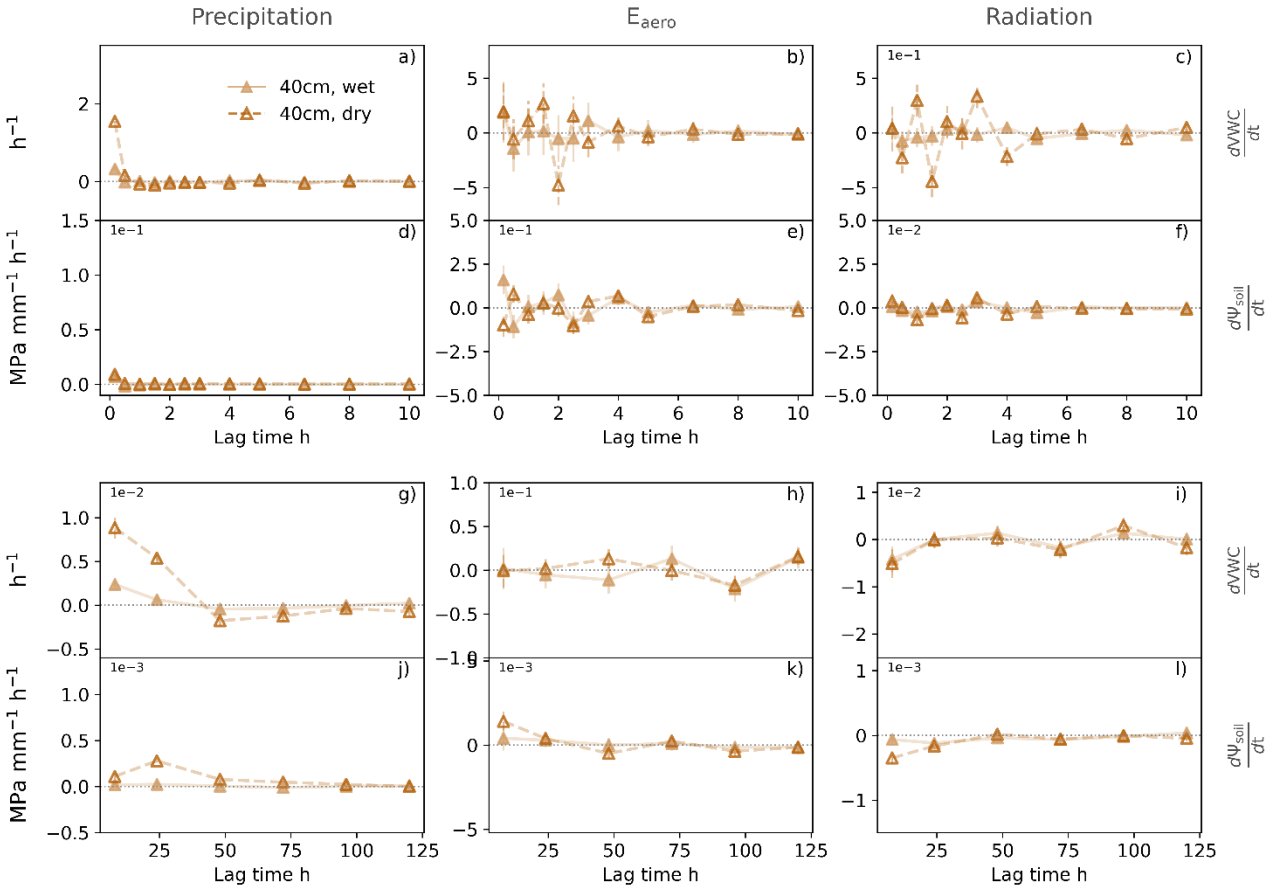

Figure C10: Beech soil cluster - Impulse responses of net soil water recharge (dVWC/dt) and net change in soil water potential (dΨsoil/dt) to impulses of precipitation (left column), Eaero (middle column) and solar radiation (right column), for 40 cm depth within the beech cluster. The upper two rows (a-f) show short-term (0-10 hour) impulse-response functions of half-hourly data, while the lower two rows (g-l) show impulse-response functions over 0-5 days. Full and empty markers show mean responses under wet and dry soil conditions, respectively, as distinguished by a threshold of -0.5 MPa in average soil water potentials at 20 cm. This threshold roughly corresponds to the 0.3-quantile of the average soil water potential at 20 cm depth measured at the beech cluster. The whiskers show +/- one standard error of the mean. Short-term responses to precipitation peak immediately, and are stronger during dry soil conditions. The short-term responses to Eaero and solar radiation are highly uncertain in the first ~5 hours. Daily responses to radiation show soil water depletion (negative net soil water recharge), as well as decreases in soil water potentials under dry soil conditions.

https://doi.org/10.5194/egusphere-2026-2481
Preprint. Discussion started: 8 May 2026

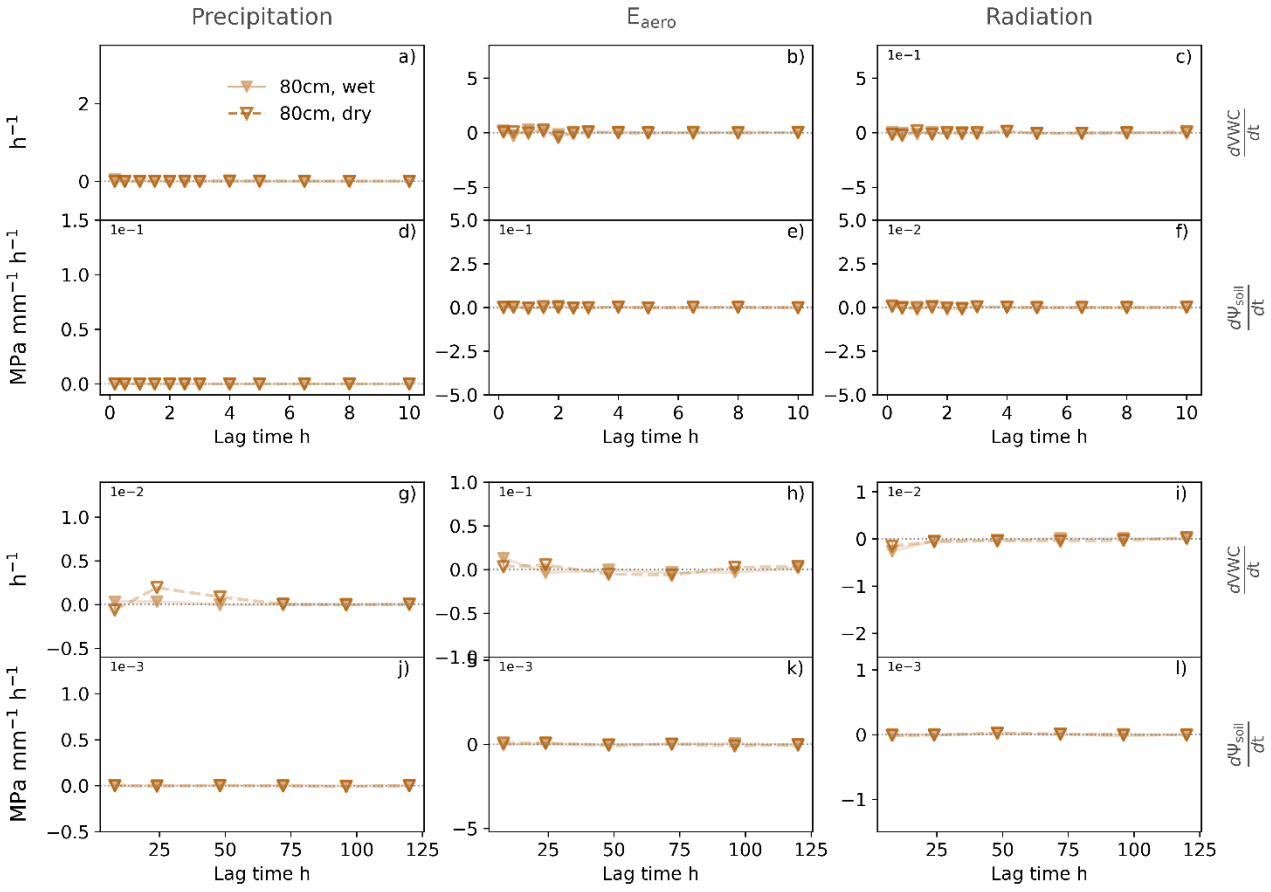

Figure C11: Beech soil cluster - Impulse responses of net soil water recharge (dVWC/dt) and net change in soil water potential (dΨsoil/dt) to impulses of precipitation (left column), Eaero (middle column) and solar radiation (right column), for 80 cm depth within the beech cluster. The upper two rows (a-f) show short-term (0-10 hour) impulse-response functions of half-hourly data, while the lower two rows (g-l) show impulse-response functions over 0-5 days. Full and empty markers show mean responses under wet and dry soil conditions, respectively, as distinguished by a threshold of -0.5 MPa in average soil water potentials at 20 cm. This threshold roughly corresponds to the 0.3-quantile of the average soil water potential at 20 cm depth measured at the beech cluster. The whiskers show +/- one standard error of the mean. Short-term responses to precipitation peak immediately, and are stronger during dry soil conditions. The short-term responses to Eaero and solar radiation are highly uncertain in the first ~5 hours. Daily responses to radiation show soil water depletion (negative net soil water recharge), as well as decreases in soil water potentials under dry soil conditions.

https://doi.org/10.5194/egusphere-2026-2481
Preprint. Discussion started: 8 May 2026

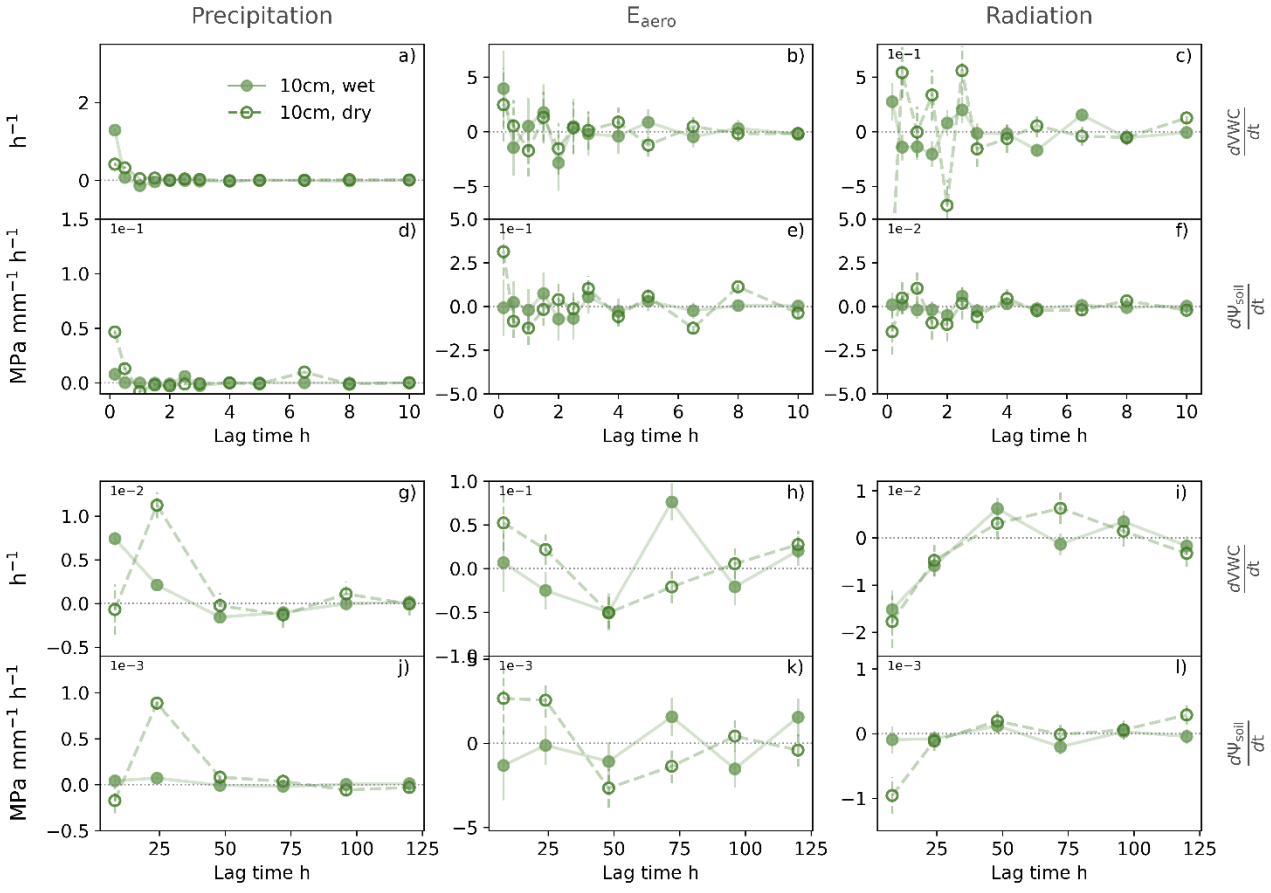

Figure C12: Spruce soil cluster - Impulse responses of net soil water recharge (dVWC/dt) and net change in soil water potential (dΨsoil/dt) to impulses of precipitation (left column), Eaero (middle column) and solar radiation (right column), for 10 cm depth within the spruce cluster. The upper two rows (a-f) show short-term (0-10 hour) impulse-response functions of half-hourly data, while the lower two rows (g-l) show impulse-response functions over 0-5 days. Full and empty markers show mean responses under wet and dry soil conditions, respectively, as distinguished by a threshold of -0.5 MPa in average soil water potentials at 20 cm. This threshold roughly corresponds to the 0.16-quantile of the average soil water potential at 20 cm depth measured at the spruce cluster. The whiskers show +/- one standard error of the mean. Short-term responses to precipitation peak immediately, and are stronger during dry soil conditions. The short-term responses to Eaero and solar radiation are highly uncertain in the first ~5 hours. Daily responses to radiation show soil water depletion (negative net soil water recharge), as well as decreases in soil water potentials under dry soil conditions.

https://doi.org/10.5194/egusphere-2026-2481
Preprint. Discussion started: 8 May 2026

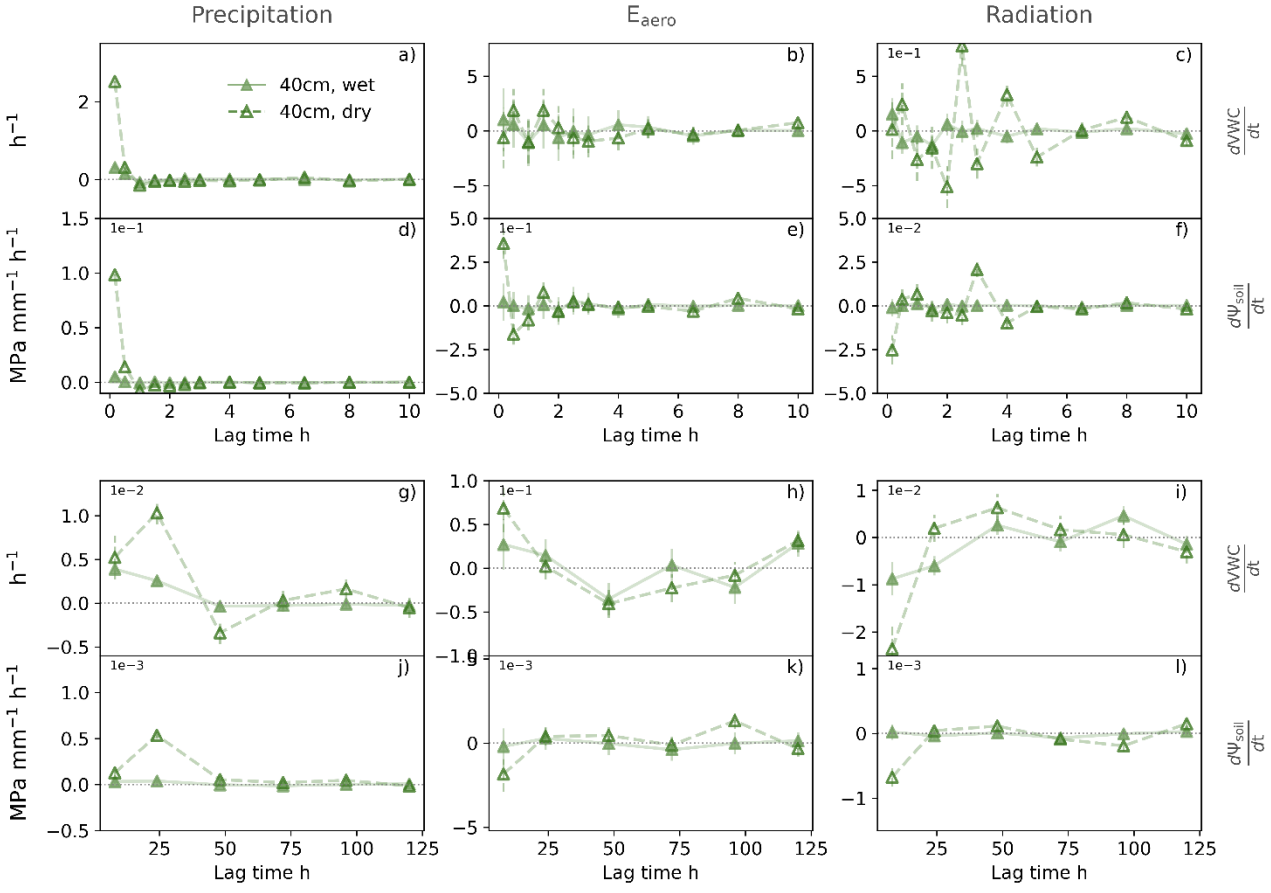

Figure C13: Spruce soil cluster - Impulse responses of net soil water recharge (dVWC/dt) and net change in soil water potential (dΨsoil/dt) to impulses of precipitation (left column), Eaero (middle column) and solar radiation (right column), for 40 cm depth within the spruce cluster. The upper two rows (a-f) show short-term (0-10 hour) impulse-response functions of half-hourly data, while the lower two rows (g-l) show impulse-response functions over 0-5 days. Full and empty markers show mean responses under wet and dry soil conditions, respectively, as distinguished by a threshold of -0.5 MPa in average soil water potentials at 20 cm. This threshold roughly corresponds to the 0.16-quantile of the average soil water potential at 20 cm depth measured at the spruce cluster. The whiskers show +/- one standard error of the mean. Short-term responses to precipitation peak immediately, and are stronger during dry soil conditions. The short-term responses to Eaero and solar radiation are highly uncertain in the first ~5 hours. Daily responses to radiation show soil water depletion (negative net soil water recharge), as well as decreases in soil water potentials under dry soil conditions.

https://doi.org/10.5194/egusphere-2026-2481
Preprint. Discussion started: 8 May 2026

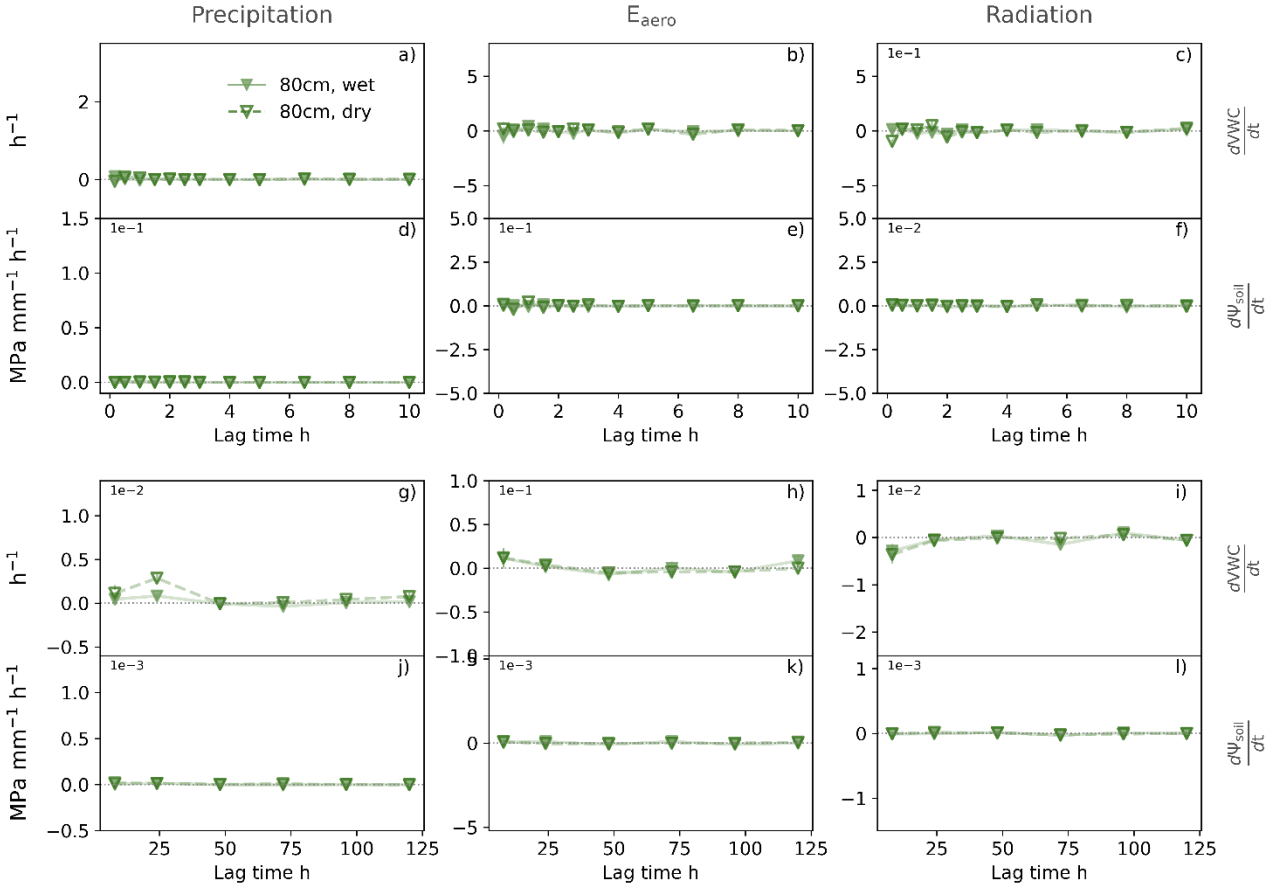

Figure C14: Spruce soil cluster - Impulse responses of net soil water recharge (dVWC/dt) and net change in soil water potential (dΨsoil/dt) to impulses of precipitation (left column), Eaero (middle column) and solar radiation (right column), for 80 cm depth within the spruce cluster. The upper two rows (a-f) show short-term (0-10 hour) impulse-response functions of half-hourly data, while the lower two rows (g-l) show impulse-response functions over 0-5 days. Full and empty markers show mean responses under wet and dry soil conditions, respectively, as distinguished by a threshold of -0.5 MPa in average soil water potentials at 20 cm. This threshold roughly corresponds to the 0.16-quantile of the average soil water potential at 20 cm depth measured at the spruce cluster. The whiskers show +/- one standard error of the mean. Short-term responses to precipitation peak immediately, and are stronger during dry soil conditions. The short-term responses to Eaero and solar radiation are highly uncertain in the first ~5 hours. Daily responses to radiation show soil water depletion (negative net soil water recharge), as well as decreases in soil water potentials under dry soil conditions.

https://doi.org/10.5194/egusphere-2026-2481
Preprint. Discussion started: 8 May 2026

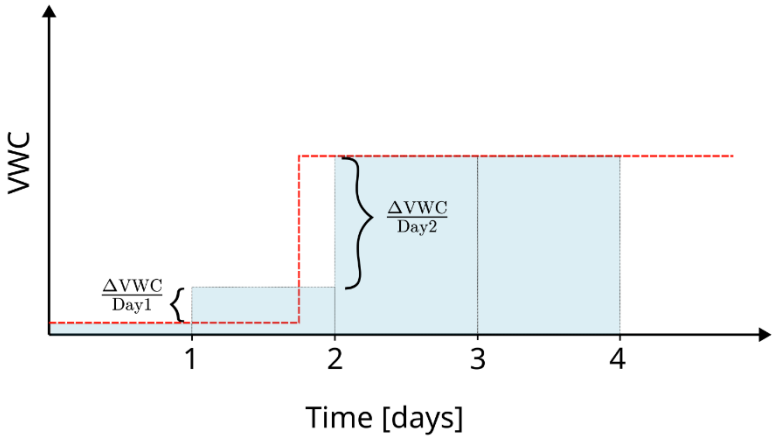

Figure C15: Example of a step change in volumetric water content (VWC, red dashed line) after precipitation occurring in the last six hours of the day. Averaging over days (blue grey rectangles) can lead to artefacts. The closer the step increase occurs at the edge of the averaging time window, the larger the artefact.

Code Availability

The R code used to calculate impulse-response functions (ERRA) is available at https://doi.org/10.16904/envidat.529 (Kirchner, 2024b).

Data Availability

The data used in this study is available on request.

https://doi.org/10.5194/egusphere-2026-2481
Preprint. Discussion started: 8 May 2026

Author Contribution

SM, PM, JWK and MGF designed the research and interpreted the results. SM and MGF collected the data and performed the analysis. JWK developed the ERRA method. SM produced the figures and wrote the initial draft of the manuscript. All authors revised and approved the manuscript.

Competing Interests

None declared.

Acknowledgements

We thank the "Waldlabor Zürich" initiative (www.waldlabor.ch) under the direction of Martin Brüllhardt, and the forest owner Jakob Heusser, for their cooperation and support. We acknowledge support in data collection and laboratory work by the technical staff and student helpers of the "WaldLab Forest Experimental Site" (Anna Lena Könz, Maria Grundmann, Lara Virsik, Elisa Hage, Mark Bühler, Gian-Luca Cavelti, Laurin Nüesch, Adrian Kreiner, Fabian Strittmatter, Ramun Bär, Martin Huber, Sasha Löffler and Lucien Biolley). We thank Harsh Beria for fruitful discussions.

Financial support

This research was funded by ETH Grant ETH-27 21-2 'Quantifying water stress at the soil-plant-atmosphere interface'

Review statement

The review statement will be added by Copernicus Publications listing the handling editor as well as all contributing referees according to their status anonymous or identified.

https://doi.org/10.5194/egusphere-2026-2481
Preprint. Discussion started: 8 May 2026

References

Allen, S. T., Kirchner, J. W., Braun, S., Siegwolf, R. T. W., and Goldsmith, G. R.: Seasonal origins of soil water used by trees, Hydrology and Earth System Sciences, 23, 1199–1210, https://doi.org/https://doi.org/10.5194/hess-23-1199-2019, 2019.

Bai, Y., Zhang, F., Ciais, P., Wigneron, J.-P., Feldman, A. F., Gentine, P., Smith, W. K., Biederman, J. A., Scott, R. L., Stoy, P. C., Yakir, D., Kemanian, A. R., Makowski, D., Yi, C., and Fu, Z.: Widespread enhancement of ecosystem carbon fluxes during post moisture pulse, Commun Earth Environ, 7, 171, https://doi.org/10.1038/s43247-026-03191-x, 2026.

Berry, J. and Bjorkman, O.: Photosynthetic Response and Adaptation to Temperature in Higher Plants, Annual Review of Plant Biology, 31, 491–543, https://doi.org/10.1146/annurev.pp.31.060180.002423, 1980.

Brodribb, T. J. and McAdam, S. A. M.: Passive Origins of Stomatal Control in Vascular Plants, Science, 331, 582–585, https://doi.org/10.1126/science.1197985, 2011.

Brodribb, T. J. and McAdam, S. A. M.: Evolution of the Stomatal Regulation of Plant Water Content, Plant Physiology, 174, 639–649, https://doi.org/10.1104/pp.17.00078, 2017.

Burns, S. P., Blanken, P. D., Turnipseed, A. A., Hu, J., and Monson, R. K.: The influence of warm-season precipitation on the diel cycle of the surface energy balance and carbon dioxide at a Colorado subalpine forest site, Biogeosciences, 12, 7349–7377, https://doi.org/10.5194/bg-12-7349-2015, 2015.

Chen, S., Xiao, J., Li, X., Wu, M., and Yang, J.: Disentangling the climate–VPD–GPP Nexus: Global patterns and underlying drivers, Global and Planetary Change, 256, 105141, https://doi.org/10.1016/j.gloplacha.2025.105141, 2026a.

Chen, W., Zhang, W., Zhu, Q., Guo, X., Zhang, J., and Jin, C.: Contrasting Effects of Hydrothermal Drivers on Gross Primary Productivity and Ecosystem Respiration, Forests, 17, 205, https://doi.org/10.3390/f17020205, 2026b.

Collins, S. L., Belnap, J., Grimm, N. B., Rudgers, J. A., Dahm, C. N., D'Odorico, P., Litvak, M., Natvig, D. O., Peters, D. C., Pockman, W. T., Sinsabaugh, R. L., and Wolf, B. O.: A Multiscale, Hierarchical Model of Pulse Dynamics in Arid-Land Ecosystems, Annual Review of Ecology, Evolution, and Systematics, 45, 397–419, https://doi.org/10.1146/annurev-ecolsys-120213-091650, 2014.

Cranko Page, J., De Kauwe, M. G., Abramowitz, G., and Pitman, A. J.: Non-Stationary Lags and Legacies in Ecosystem Flux Response to Antecedent Rainfall, Journal of Geophysical Research: Biogeosciences, 128, e2022JG007144, https://doi.org/10.1029/2022JG007144, 2023.

Delgado-Balbuena, J., Loescher, H. W., Aguirre-Gutiérrez, C. A., Alfaro-Reyna, T., Pineda-Martínez, L. F., Vargas, R., and Arredondo, T.: Dynamics of short-term ecosystem carbon fluxes induced by precipitation events in a semiarid grassland, Biogeosciences, 20, 2369–2385, https://doi.org/10.5194/bg-20-2369-2023, 2023.

https://doi.org/10.5194/egusphere-2026-2481
Preprint. Discussion started: 8 May 2026

Feldman, A. F., Short Gianotti, D. J., Konings, A. G., McColl, K. A., Akbar, R., Salvucci, G. D., and Entekhabi, D.: Moisture pulse-reserve in the soil-plant continuum observed across biomes, Nature Plants, 4, 1026–1033, https://doi.org/10.1038/s41477-018-0304-9, 2018.

Feldman, A. F., Chulakadabba, A., Short Gianotti, D. J., and Entekhabi, D.: Landscape-Scale Plant Water Content and Carbon Flux Behavior Following Moisture Pulses: From Dryland to Mesic Environments, Water Resources Research, 57, e2020WR027592, https://doi.org/10.1029/2020WR027592, 2021a.

Feldman, A. F., Short Gianotti, D. J., Konings, A. G., Gentine, P., and Entekhabi, D.: Patterns of plant rehydration and growth following pulses of soil moisture availability, Biogeosciences, 18, 831–847, https://doi.org/10.5194/bg-18-831-2021, 2021b.

Floriancic, M. G., Allen, S. T., and Kirchner, J. W.: Isotopic evidence for seasonal water sources in tree xylem and forest soils, Ecohydrology, 17, e2641, https://doi.org/10.1002/eco.2641, 2024.

Fu, L., Tan, J., Lysenko, V., and Guo, Y.: Disentangling the relative effects of solar radiation and vapor pressure deficit on ecosystem photosynthetic efficiency based on global eddy-covariance observations, Plant Ecol, 226, 1239–1250, https://doi.org/10.1007/s11258-025-01563-5, 2025.

Gao, H., Pfister, L., and Kirchner, J. W.: Quantifying controls on rapid and delayed runoff response in double-peak hydrographs using ensemble rainfall-runoff analysis (ERRA), Hydrology and Earth System Sciences, 29, 6529–6547, https://doi.org/10.5194/hess-29-6529-2025, 2025a.

Gao, H., Ju, Q., Zhang, D., Wang, Z., Hao, Z., and Kirchner, J. W.: Quantifying Dynamic Linkages Between Precipitation, Groundwater Recharge, and Streamflow Using Ensemble Rainfall-Runoff Analysis, Water Resources Research, 61, e2024WR037821, https://doi.org/10.1029/2024WR037821, 2025b.

Gebhardt, T., Hesse, B. D., Hikino, K., Kolovrat, K., Hafner, B. D., Grams, T. E. E., and Häberle, K.-H.: Repeated summer drought changes the radial xylem sap flow profile in mature Norway spruce but not in European beech, Agricultural and Forest Meteorology, 329, 109285, https://doi.org/10.1016/j.agrformet.2022.109285, 2023.

Grant, R. F., Desai, A. R., and Sulman, B. N.: Modelling contrasting responses of wetland productivity to changes in water table depth, Biogeosciences, 9, 4215–4231, https://doi.org/10.5194/bg-9-4215-2012, 2012.

Grossiord, C., Buckley, T. N., Cernusak, L. A., Novick, K. A., Poulter, B., Siegwolf, R. T. W., Sperry, J. S., and McDowell, N. G.: Plant responses to rising vapor pressure deficit, New Phytologist, 226, 1550–1566, https://doi.org/10.1111/nph.16485, 2020.

Hesse, B. D., Gebhardt, T., Hafner, B. D., Hikino, K., Reitsam, A., Gigl, M., Dawid, C., Häberle, K.-H., and Grams, T. E. E.: Physiological recovery of tree water relations upon drought release—response of mature beech and spruce after five years of recurrent summer drought, Tree Physiology, tpac135, https://doi.org/10.1093/treephys/tpac135, 2022.

https://doi.org/10.5194/egusphere-2026-2481
Preprint. Discussion started: 8 May 2026

Huxman, T. E., Snyder, K. A., Tissue, D., Leffler, A. J., Ogle, K., Pockman, W. T., Sandquist, D. R., Potts, D. L., and Schwinning, S.: Precipitation pulses and carbon fluxes in semiarid and arid ecosystems, Oecologia, 141, 254–268, https://doi.org/10.1007/s00442-004-1682-4, 2004a.

Huxman, T. E., Cable, J. M., Ignace, D. D., Eilts, J. A., English, N. B., Weltzin, J., and Williams, D. G.: Response of net ecosystem gas exchange to a simulated precipitation pulse in a semi-arid grassland: the role of native versus non-native grasses and soil texture, Oecologia, 141, 295–305, https://doi.org/10.1007/s00442-003-1389-y, 2004b.

Jones, H. G. and Sutherland, R. A.: Stomatal control of xylem embolism, Plant, Cell & Environment, 14, 607–612, https://doi.org/10.1111/j.1365-3040.1991.tb01532.x, 1991.

Kannenberg, S. A., Novick, K. A., and Phillips, R. P.: Anisohydric behavior linked to persistent hydraulic damage and delayed drought recovery across seven North American tree species, New Phytologist, 222, 1862–1872, https://doi.org/10.1111/nph.15699, 2019.

Kirchner, J. W.: Impulse Response Functions for Nonlinear, Nonstationary, and Heterogeneous Systems, Estimated by Deconvolution and Demixing of Noisy Time Series, Sensors, 22, 3291, https://doi.org/10.3390/s22093291, 2022.

Kirchner, J. W.: Characterizing nonlinear, nonstationary, and heterogeneous hydrologic behavior using ensemble rainfall–runoff analysis (ERRA): proof of concept, Hydrology and Earth System Sciences, 28, 4427–4454, https://doi.org/10.5194/hess-28-4427-2024, 2024.

ERRA -- an R script for Ensemble Rainfall-Runoff Analysis.:

Knapp, J. L. A., Berghuijs, W. R., Floriancic, M. G., and Kirchner, J. W.: Catchment hydrological response and transport are affected differently by precipitation intensity and antecedent wetness, Hydrology and Earth System Sciences, 29, 3673–3685, https://doi.org/10.5194/hess-29-3673-2025, 2025.

Knüver, T., Bär, A., Ganthaler, A., Gebhardt, T., Grams, T. E. E., Häberle, K.-H., Hesse, B. D., Losso, A., Tomedi, I., Mayr, S., and Beikircher, B.: Recovery after long-term summer drought: Hydraulic measurements reveal legacy effects in trunks of Picea abies but not in Fagus sylvatica, Plant Biology, 24, 1240–1253, https://doi.org/10.1111/plb.13444, 2022.

Liu, Z., Liu, Z., Jia, G., Yu, X., Meng, J., and Yuan, C.: Soil water mixing dynamics and plant hydraulic regulation determine water transport time lags within the soil–plant continuum, Ecological Frontiers, 46, 325–332, https://doi.org/10.1016/j.ecofro.2025.09.012, 2026.

Ma, Y., Liu, H., Zhao, W., Guo, L., Yang, Q., Li, Y., Liu, J., and Yetemen, O.: Responses of Soil Water Potential and Plant Physiological Status to Pulsed Rainfall Events in Arid Northwestern China: Implications for Disclosing the Water-Use Strategies of Desert Plants, Ecohydrology, 18, e2728, https://doi.org/10.1002/eco.2728, 2025.

Martinetti, S., Molnar, P., Carminati, A., and Floriancic, M. G.: Contrasting the soil–plant hydraulics of beech and spruce by linking root water uptake to transpiration dynamics, Tree Physiology, 45, tpae158, https://doi.org/10.1093/treephys/tpae158, 2025.

https://doi.org/10.5194/egusphere-2026-2481
Preprint. Discussion started: 8 May 2026

Martinetti, S., Carminati, A., Molnar, P., and Floriancic, M. G.: The interplay between hydraulic capacitance and stomatal regulation strategy affects soil–plant hydraulics and transpiration, New Phytologist, n/a, https://doi.org/10.1111/nph.71143, 2026.

McAdam, S. A. M. and Brodribb, T. J.: Separating Active and Passive Influences on Stomatal Control of Transpiration, Plant Physiol, 164, 1578–1586, https://doi.org/10.1104/pp.113.231944, 2014.

McAdam, S. A. M. and Brodribb, T. J.: The Evolution of Mechanisms Driving the Stomatal Response to Vapor Pressure Deficit, Plant Physiol, 167, 833–843, https://doi.org/10.1104/pp.114.252940, 2015.

Paschalis, A., Fatichi, S., Katul, G. G., and Ivanov, V. Y.: Cross-scale impact of climate temporal variability on ecosystem water and carbon fluxes, Journal of Geophysical Research: Biogeosciences, 120, 1716–1740, https://doi.org/10.1002/2015JG003002, 2015.

Peters, R. L., Pappas, C., Hurley, A. G., Poyatos, R., Flo, V., Zweifel, R., Goossens, W., and Steppe, K.: Assimilate, process and analyse thermal dissipation sap flow data using the TREX r package, Methods in Ecology and Evolution, 12, 342–350, https://doi.org/10.1111/2041-210X.13524, 2021.

Piayda, A., Dubbert, M., Siegwolf, R., Cuntz, M., and Werner, C.: Quantification of dynamic soil–vegetation feedbacks following an isotopically labelled precipitation pulse, Biogeosciences, 14, 2293–2306, https://doi.org/10.5194/bg-14-2293-2017, 2017.

Qi, S., Wang, G., Li, W., Xiang, D., Zhou, S., and Lv, Z.: Soil Depth Matters: Divergent Drivers of Ecosystem Productivity in Alpine Ecosystems, Global Ecology and Biogeography, 34, e70071, https://doi.org/10.1111/geb.70071, 2025.

Roby, M. C., Scott, R. L., and Moore, D. J. P.: High Vapor Pressure Deficit Decreases the Productivity and Water Use Efficiency of Rain-Induced Pulses in Semiarid Ecosystems, Journal of Geophysical Research: Biogeosciences, 125, e2020JG005665, https://doi.org/10.1029/2020JG005665, 2020.

Rodriguez-Dominguez, C. M., Buckley, T. N., Egea, G., de Cires, A., Hernandez-Santana, V., Martorell, S., and Diaz-Espejo, A.: Most stomatal closure in woody species under moderate drought can be explained by stomatal responses to leaf turgor, Plant, Cell & Environment, 39, 2014–2026, https://doi.org/10.1111/pce.12774, 2016.

Schlesinger, W. H. and Jasechko, S.: Transpiration in the global water cycle, Agricultural and Forest Meteorology, 189–190, 115–117, https://doi.org/10.1016/j.agrformet.2014.01.011, 2014.

Sharma, R. P., Vacek, Z., and Vacek, S.: Individual tree crown width models for Norway spruce and European beech in Czech Republic, Forest Ecology and Management, 366, 208–220, https://doi.org/10.1016/j.foreco.2016.01.040, 2016.

Shimazaki, K., Doi, M., Assmann, S. M., and Kinoshita, T.: Light Regulation of Stomatal Movement, Annual Review of Plant Biology, 58, 219–247, https://doi.org/10.1146/annurev.arplant.57.032905.105434, 2007.

Ulrich, D. E. M. and Grossiord, C.: Faster drought recovery in anisohydric beech compared with isohydric spruce, Tree Physiology, 43, 517–521, https://doi.org/10.1093/treephys/tpad009, 2023.

https://doi.org/10.5194/egusphere-2026-2481
Preprint. Discussion started: 8 May 2026

Wang, L., Manzoni, S., Ravi, S., Riveros-Iregui, D., and Caylor, K.: Dynamic interactions of ecohydrological and biogeochemical processes in water-limited systems, Ecosphere, 6, art133, https://doi.org/10.1890/ES15-00122.1, 2015.

Wang, Z., Slot, M., and Wang, C.: Decoupling of stomatal conductance, transpiration and photosynthesis in terrestrial plants under elevated temperature: a meta-analysis, Nat Commun, 17, 1528, https://doi.org/10.1038/s41467-025-68250-x, 2026.

Wankmüller, F. J. P., Delval, L., Lehmann, P., Baur, M. J., Cecere, A., Wolf, S., Or, D., Javaux, M., and Carminati, A.: Global influence of soil texture on ecosystem water limitation, Nature, 635, 631–638, https://doi.org/10.1038/s41586-024-08089-2, 2024.

Werner, C., Meredith, L. K., Ladd, S. N., Ingrisch, J., Kübert, A., van Haren, J., Bahn, M., Bailey, K., Bamberger, I., Beyer, M., Blomdahl, D., Byron, J., Daber, E., Deleeuw, J., Dippold, M. A., Fudyma, J., Gil-Loaiza, J., Honeker, L. K., Hu, J., Huang, J., Klüpfel, T., Krechmer, J., Kreuzwieser, J., Kühnhammer, K., Lehmann, M. M., Meeran, K., Misztal, P. K., Ng, W.-R., Pfannerstill, E., Pugliese, G., Purser, G., Roscioli, J., Shi, L., Tfaily, M., and Williams, J.: Ecosystem fluxes during drought and recovery in an experimental forest, Science, 374, 1514–1518, https://doi.org/10.1126/science.abj6789, 2021.

Williams, C. A., Hanan, N., Scholes, R. J., and Kutsch, W.: Complexity in water and carbon dioxide fluxes following rain pulses in an African savanna, Oecologia, 161, 469–480, https://doi.org/10.1007/s00442-009-1405-y, 2009.

Zeppel, M., Macinnis-Ng, C. M. O., Ford, C. R., and Eamus, D.: The response of sap flow to pulses of rain in a temperate Australian woodland, Plant Soil, 305, 121–130, https://doi.org/10.1007/s11104-007-9349-7, 2008.

Zhou, S., Williams, A. P., Berg, A. M., Cook, B. I., Zhang, Y., Hagemann, S., Lorenz, R., Seneviratne, S. I., and Gentine, P.: Land–atmosphere feedbacks exacerbate concurrent soil drought and atmospheric aridity, Proceedings of the National Academy of Sciences, 116, 18848–18853, https://doi.org/10.1073/pnas.1904955116, 2019.

Zweifel, R., Zimmermann, L., and Newbery, D. M.: Modeling tree water deficit from microclimate: an approach to quantifying drought stress, Tree Physiology, 25, 147–156, https://doi.org/10.1093/treephys/25.2.147, 2005.